# HYDRA – A 3-DIMENSIONAL ELECTRON AND ION HOT PLASMA INSTRUMENT FOR THE POLAR SPACECRAFT OF THE GGS MISSION

J. SCUDDER
*University of Iowa, Iowa City, Iowa, 52242, U.S.A.*

F. HUNSACKER, G. MILLER, J. LOBELL, T. ZAWISTOWSKI, K. OGILVIE, J. KELLER, D. CHORNAY, F. HERRERO, R. FITZENREITER and D. FAIRFIELD
*Laboratory for Extraterrestrial Physics, NASA Goddard Space Flight Center, Greenbelt, MD 20771, U.S.A.*

J. NEEDELL, D. BODET, J. GOOGINS, C. KLETZING and R. TORBERT
*University of New Hampshire, Durham, New Hampshire, U.S.A.*

J. VANDIVER
*Vandiver Associates, Huntsville, Alabama, U.S.A.*

R. BENTLEY, W. FILLIUS, C. McILWAIN and E. WHIPPLE
*UCSD, La Jolla, California, U.S.A.*

and

A. KORTH
*MPAE, Katlenberg-Lindau, Germany*

(Received 30 October, 1993)

**Abstract.** HYDRA is an experimental hot plasma investigation for the POLAR spacecraft of the GGS program. A consortium of institutions has designed a suite of particle analyzers that sample the velocity space of electron and ions between $\simeq$ 2 keV/$q$ – 35 keV/$q$ in three dimensions, with a routine time resolution of 0.5 s. Routine coverage of velocity space will be accomplished with an angular homogeneity assumption of $\simeq 16°$, appropriate for subsonic plasmas, but with special $\simeq 1.5°$ resolution for electrons with energies between 100 eV and 10 keV along and opposed to the local magnetic field. This instrument produces 4.9 kilobits $s^{-1}$ to the telemetry, consumes on average 14 W and requires 18.7 kg for deployment including its internal shielding. The scientific objectives for the polar magnetosphere fall into four broad categories: (1) those to define the ambient kinetic regimes of ions and electrons; (2) those to elucidate the magnetohydrodynamic responses in these regimes; (3) those to assess the particle populations with high time resolution; and (4) those to determine the global topology of the magnetic field. In the *first* group are issues of identifying the origins of particles at high magnetic latitudes, their energization, the altitude dependence of the forces, including parallel electric fields they have traversed. In the *second* group are the physics of the fluid flows, regimes of current, and plasma depletion zones during quiescent and disturbed magnetic conditions. In the *third* group is the exploration of the processes that accompany the rapid time variations known to occur in the auroral zone, cusp and entry layers as they affect the flow of mass, momentum and energy in the auroral region. In the *fourth* class of objectives are studies in conjunction with the SWE measurements of the Strahl in the solar wind that exploit the small gyroradius of thermal electrons to detect those magnetic field lines that penetrate the auroral region that are directly 'open' to interplanetary space where, for example, the Polar Rain is observed.

*Space Science Reviews* **71:** 459–495, 1995.

## 1. Introduction

For many years the phenomena of the Earth's auroral magnetosphere have challenged our understanding of cause and effect in solar terrestrial physics. The enormous concentration in the polar region of magnetic field lines from many different locales of the magnetosphere makes this region highly structured in space and the focal point for many signatures of time dependent relaxation of the magnetosphere as a whole. Routine time, configuration space. velocity space, and compositional coverage have not always been simultaneously available as diagnostics for these processes. The POLAR spacecraft instrument complement together with those of the other GGS vehicles and the FAST SMEX spacecraft are soon to mount a multipoint attack on this global problem. The polar magnetosphere is the ultimate kinetic regime driven by external MHD exigencies. The solar wind impresses a changing external emf across a highly structured, magnetized and conducting ionosphere, forcing currents and reorganization of field lines and even magnetic topologies. This plasma regime is not one that can be understood by MHD orderings, and requires a thorough and as nearly model independent kinetic assessment of the plasma as technology can permit.

The presently described HYDRA hot plasma investigation was proposed in response to these varying demands for further information about such a complicated system. The experimental approach follows the successful ISEE VES (Ogilvie *et al.*, 1978) concept of sampling the plasma velocity distribution function with as close to delta function resolution in velocity space, consistent with adequate statisitics and $\simeq 0.5$ s time resolution. In this way the telemetered information of the velocity distribution of electrons and ions along the sampled fields of view is an engineering quantity, *not* a deconvolution product. Because the plasma in these regimes is primarily 'hot' in the sense that its random energy is much larger than its bulk energy, the entire $4\pi$ of velocity space must be routinely sampled in a non-aliased way, while covering an energy range suitable to inventory typical thermal and suprathermal populations. The intrinsically kinetic nature of the entire magnetosphere viewed as a plasma sheath implies that a variety of velocity space structures (for example ion conics, inverted 'V's', and modifications of the loss cone with $E_{||}$) must be anticipated and provisions made for their resolution. The dynamic and unpredictable nature of the magnetospheric system with substorms and other forms of geomagnetic activity as well as the anticipated swift spacecraft traversals of field aligned structures at low altitude, drives the experimental approach to simultaneously sample multiple directions on the unit sphere at the *same* time so that the experiment's time resolution is determined by the energy sweep time of the analyzer (0.5 s), rather than the spacecraft rotation period which is limited by the dynamics of booms and appendages.

## 2. Instrument Description

The HYDRA instrumentation is deployed in five separate packages mounted at various locations on the GGS/Polar spacecraft as indicated in Figure 1. These are the Data Processing Unit (DPU), two sets of 127° electrostatic analyzers (ESA's) called the DDEIS, and two parallel plate imaging analyzers called the PPA. All the boxes except the DPU are dispersed about the perimeter of the two instrument shelves. These electro-optical sensor packages are separated by 180° in spacecraft phase or roll angle from their mirror symmetric partner as illustrated in the top view of this figure. The shelf location of a given box was dictated by the proximity of other spacecraft appendages and the need for a clear field of view of the various sensors. The separate boxes of HYDRA are logically interconnected as indicated by the block diagram of Figure 2. Other logical and physically distinct structures within the DDEIS boxes themselves are also indicated: each box has their own (i) low voltage power converter, (ii) dedicated electron and ion channeltron bias supplies, (iii) bi-polar, dual range stepping power supply, and (iv) intra-instrument interface card. The DPU has its own power converter. The DPU is mounted inboard away from the spacecraft skin on the underside of the upper instrument shelf as indicated in the isometric drawings in Figure 1. For the convenience of its central location, the UV calibration lamp is mounted on top of the DPU box.

The first pair of diagonally opposed electro-optical sensor units is the DuoDeca Electron Spectrometer (DDEIS) which contains 12 narrow (10° FW) fields of views (defined by 127° cylindrical ESA's) dispersed across the unit sphere to sample electrons and ions. The second pair of diagonally opposed sensors comprise the Parallel Plate Analyzer (PPA) each with a conical (30° FW) field of view subtending 1024 (1.5° × 1.5°) pixels of a position sensitive detector. The energy selection of the PPA is accomplished by a parallel plate ESA; it samples electrons with a much higher anglar resolution than the ESA s of the DDEIS assembly. The individual ESA's of the DDEIS unit 1 and the center line of the PPA unit 1 are pointed downwards (labeled 'down') and parallel to the spacecraft spin equator, respectively. These two boxes are located at the spacecraft perimeter on the lower side of the lower equipment deck as shown in FiguTe 1. An isometric view of one half of the DDEIS is shown in Figure 3. The radially opposed ESA's of the DDEIS unit 2 and the symmetry axis of the PPA unit 2 are aimed 'above' and parallel to the spacecraft spin equator, respectively. These two boxes are attached to the upper side of the upper equipment deck as illustrated in Figure 1. This deployment scheme provides 6 pairs of instantaneously collinear mean FOV's (in velocity space) for the ESA's of the DDEIS and 1024 pairs of instantaneously anti-collinear (in velocity space) FOV pixels within the PPA units.

Loss/source cone and ancillary angular coverage at the same energy as that in the field directions is obtained for electrons with a pair of imaging class, body mounted modified Parallel Plate Analyzers that form the PPA. They possess a $\Delta E/E \simeq 20\%$, with a geometrical factor of $1.1 \times 10^{-3} E$/keV cm$^2$ strd pixel$^{-1}$.

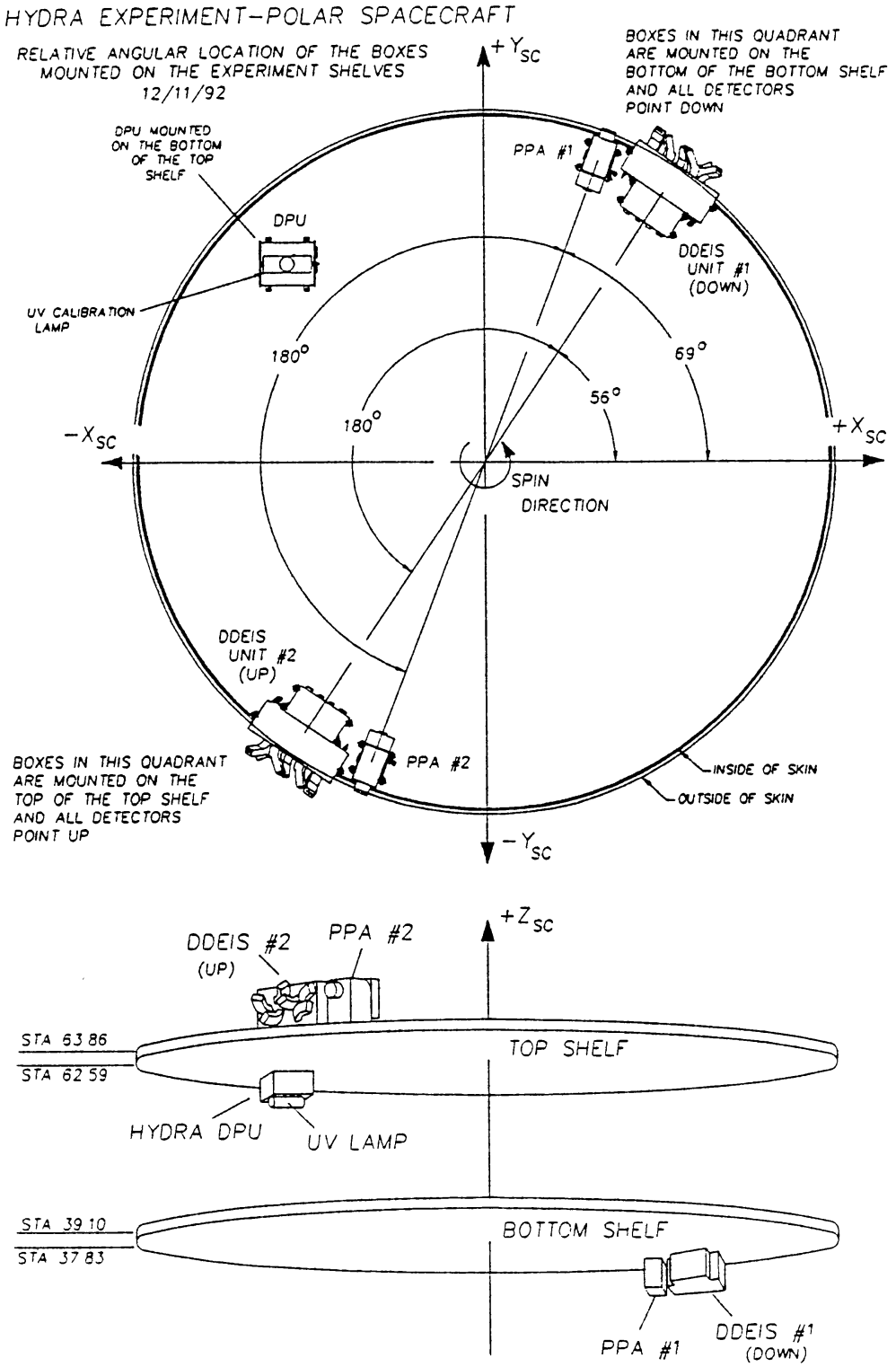


Fig. 1. Shelf Isometric of Spacecraft Equipment Decks locating HYDRA boxes. CircullIferential solar panels have been removed. Despun platform has also not been included.

Depending on the precise orientation of the magnetic field in spacecraft coordinates, between 30 and 3000 pixels contribute to a given pitch-angle bucket per spin. The telemetered pitch-angle resolution is variable, and is non-uniformly spaced across 0°, 180°. The partition of the allocated telemetery from the accumulators

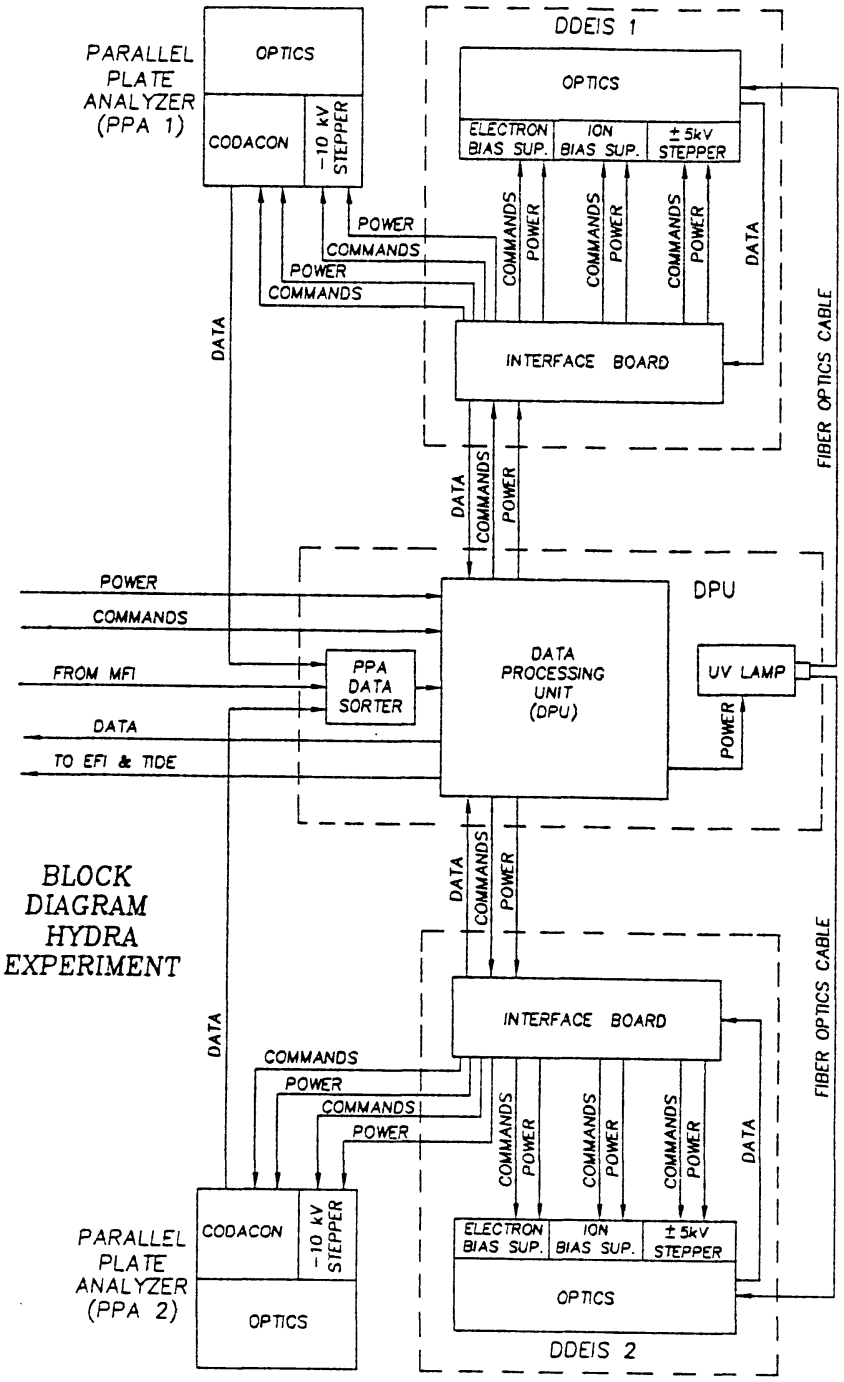


Fig. 2. Block Diagram of HYDRA.

can be changed by command. The higher angular resolution afforded by the PPA is acquired during one half spin period of the spacecraft. The DPU controlled unipolar stepping supply of the PPA electron-optics has several energies where the transmitted particles are of the same energy as that of the DDEIS sensors, allowing cross calibration. It is foreseen that the DDEIS electron morphology may be queried by the DPU to 'servo' the slower PPA acquisition to the 'interesting' energy regions where higher angular resolution is required.

The circular collimator at the aperture of the PPA units and the entire face plates of the DDEIS as well as parts of the ESA assemblies protrude through the spacecraft circumference (cf. Figure 1) that is otherwise covered with solar array glass. The exposed surface of the DDEIS is coated with electrically conductive NASA-GSFC Goddard green paint (NS-53B). The exposed PPA aperture is treated with adequately conductive Dow 9 coating (Mil Spec M-3171). There are no known obstructions in the FOV's of any of the HYDRA sensors.

Deployed in this manner HYDRA performs a simultaneous, (fore and aft), dense, survey of $4\pi$ strd (including loss cone coverage) on each energy level to which it is tuned. As the spacecraft rotates and the analyzers are simultaneously tuned to transmit successive energies, a survey is obtained in 0.5 s of the three dimensional energy-angle distribution function, $f(\mathbf{v})$, including the loss cone. As homogeneous conditions in space and time permit, multiple energy sweeps can be superposed on the ground to obtain maximal velocity space angular resolution including survey of the loss cone on a time scale of 3 s. Such angular, speed and time-spatial resolution of $f(\mathbf{v}, t(\mathbf{x}))$ allow nearly model independent moment determinations of the magnetohydrodynamic regimes of our investigation in a particularly facile way. Of course knowledge of $f(\mathbf{v})$ implies the ability to synthesize pitch-angle distributions of ions and electrons as well-allowing local inferences of the 'origins' of plasmas in the Earth's environment detected within different regimes of phase space discussed by Whipple (1978) and Mizera and Fennel (1977), for example.

### 2.1. Properties of the DuoDeca electron ion spectrometer: DDEIS

The DuoDeca Electron Ion Spectrometer (DDEIS) design concept is an outgrowth of the GSFC's OGO- 5 Electron Spectrometer and ISEE-1 Vector Electron Spectrometer (VES) instruments described previously (Ogilvie et al, 1978). The ISEE VES instrument was and the GGS/WIND SWE VEIS is also comprised of two packages each containing three (3) 127° cylindrical electrostatic analyzers (cf., Ogilvie *et al.*, 1994). For every analyzer in package 1 of the VES there was deployed another 127° analyzer in package 2 with anti-collinear velocity space fields of view. In this way the VES was comprised of 3 pairs of anti-collinear narrow fields of view in velocity space defined by the 127° cylindrical ESA's of the ISEE balanced plate design; in addition each axis of a given pair was mutually orthogonal to every other. By contrast, the DDEIS of HYDRA is comprised of six pairs of unencumbered anti-collinear fields of view, each of the two boxes of the DDEIS having six ESA's as illustrated in Figure 3. Conflicts of clear field of view have precluded HYDRA's DDEIS from having its originally intended orthonormal subset of anti-collinear fields of view. This requires a generalized approach to the fluid moment analysis that is discussed below.

The instantaneous fields of view of HYDRA are indicated in the equal area projection of Figure 4. As the spacecraft spins the repeated energy sweeps of the ESA's 'fill-in' the shaded latitudinal belts of velocity space at the expense of

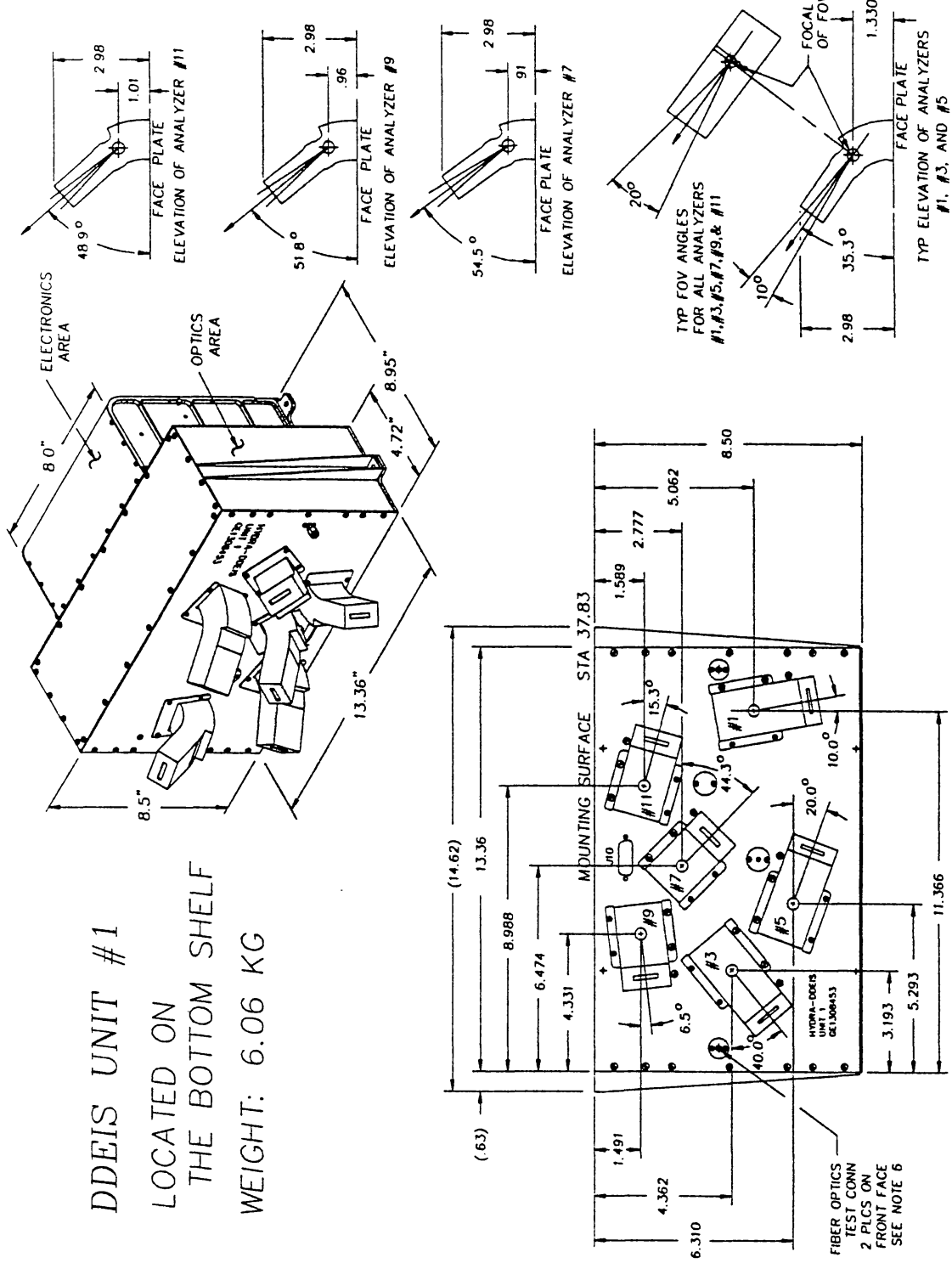


Fig. 3. DDEIS Unit 1, 'Up' Isometric Box. ESA analyzers project trhough the flat outer plate of box which is a secant facet on the spacecraft perimeter. The plate and exposed extremities of ESA's are painted with conductive paint as described in the text. The curved electronics area encloses the interface board, bias and stepping supplies of Figure 2. tte rectangular box contains the ensemble of electro-optics and their channeltrons.

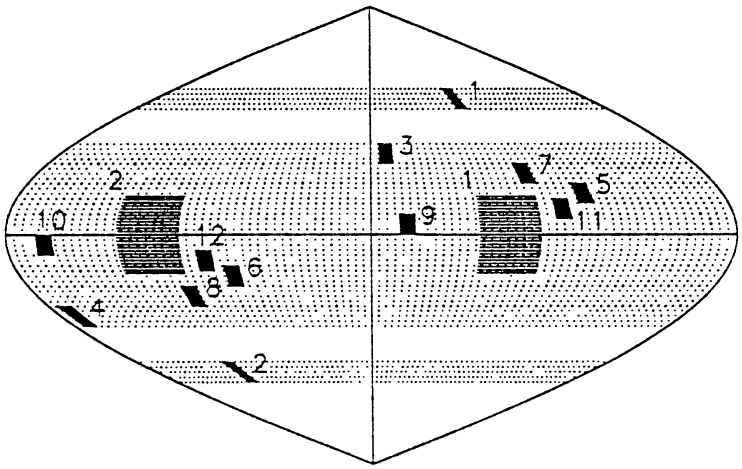


Fig. 4. Equal Area Unit Sphere Projections (spots) of instantaneous samples, (shaded region) after one spin.

time resolution. The PPA, together with the on board sorter board portion of the DPU (described below) provides high angular resolution pitch-angle distributions from a swath of viewing directions about the equator of the spacecraft; the Polar spacecraft's orbit and atitude were designed to place the geomagnetic field in the spacecraft's spin equator. Thus, each PPA sensor is foreseen to pass through 0° pitch angle once per spin, giving more than 30 separate pixels in the PPA's 'compound eye' an opportunity to sample the most singular field directions on a given rotation.

The mechanical deployment of the DDEIS optics provides for each ESA a simultaneous mean field of view in spacecraft polar angles given by columns 2 and 3 from Table I.

Zero spacecraft latitude ($\theta = 0$) is the $+z$ axis, the direction of the spin angular momentum vector. The zero of the $\phi$ coordinate corresponds to the spacecraft $+x$ axis, which is aligned with the magnetometer boom. The symmetry axis of the of the bore sight of the PPA sensors numbered (1;2) are located at ($\theta$, $\phi$) = (90°, 69°); (90°, 249°), respectively. The accepted particles have direction cosines that are opposite to that of the fields of view implied by the above table.

Separate, permanently biased. funnel shaped, ceramic Sjuts channeltrons are the sensitive elements for electrons and ions at the exit plane of each ESA' s as illustrated in breakaway section in Figure 5. The actual mean field of view for a each channeltron within a given ESA analyzer is offset slightly from the mean viewing angle given by the first two columns of Table I which are the center of the band-pass of the electro-optical system without consideration for where the flux stikes a sensor on the exit plane. The relevant offsets have been measured after assembly and are indicated in the right most pairs of columns in Table I; those mean FOV polar angles for ions are indicated by $\langle\,\rangle_+$ and those for electrons by $\langle\,\rangle_-$.

TABLE I

Hydra geometry constants

| ESA | $\langle\theta_{S/C}\rangle$ | $\langle\phi_{S/C}\rangle$ | $\langle\theta_{S/C}\rangle_+$ | $\langle\phi_{S/C}\rangle_+$ | $\langle\theta_{S/C}\rangle_-$ | $\langle\phi_{S/C}\rangle_-$ |
|---|---|---|---|---|---|---|
| 1 | 143.49 | 69.78 | 144.17 | 65.53 | 142.66 | 73.88 |
| 2 | 36.51 | 249.78 | 37.34 | 253.88 | 35.83 | 245.53 |
| 3 | 121.64 | 8.75 | 119.30 | 7.45 | 123.97 | 10.11 |
| 4 | 58.36 | 188.75 | 56.03 | 190.11 | 60.70 | 187.45 |
| 5 | 106.21 | 109.00 | 108.75 | 108.44 | 103.66 | 109.55 |
| 6 | 73.79 | 289.00 | 76.34 | 289.55 | 71.25 | 288.44 |
| 7 | 113.93 | 83.04 | 115.95 | 81.25 | 111.88 | 84.29 |
| 8 | 66.07 | 263.04 | 68.12 | 264.79 | 64.05 | 261.25 |
| 9 | 94.01 | 17.98 | 91.42 | 17.75 | 96.60 | 18.21 |
| 10 | 85.99 | 197.98 | 83.40 | 198.21 | 88.58 | 197.75 |
| 11 | 99.99 | 96.08 | 102.54 | 95.54 | 97.44 | 96.61 |
| 12 | 80.01 | 276.08 | 82.56 | 276.61 | 77.46 | 275.54 |

The economies of fabrication of the ESA assemblies implies that the fields of view of the channeltrons of the same polarity in the same anticollinear pair of ESA's are not quite anti-collinear. The departure from collinearity for a given species within a pair is 5.2°.

Behind each 127° analyzer are two channeltrons that are continuously, but separately, biased for ion and electron detection (cf., Figures 5 and 6). These customized channeltrons, provided by Sjuts in collaboration with MPAE Lindau, are compact rectangular (8 × 13.5 × 27.8) mm parallelapiped shaped ceramic with a sinuous channel formed in the ceramic which is then deposited with glass. A cross section of these channeltrons is indicated in Figure 8. These compact channeltrons and their associated amplifiers are located in a 'coffin' designed to shield a minimum volume of the channeltrons and their amplifiers against the otherwise significant penetrating particle radiation that confront all instruments on the POLAR spacecraft. This 'coffin' assembly is also depicted in Figure 5. Portions of the shield are formed by the stainless steel outer plate in the ESA which protects the channeltron from direct access 'through' the exposed ESA horn. while other equivalent thicknesses of aluminum form barriers around the channeltrons proper (cf., Figure 5). The spacecraft interior also provides shielding from the rear of the package. In this way our ability is enhanced to identify the telemetered counts with particles that have been selected in energy and angle by the ESA proper, rather than with penetrating radiation which has bypassed the energy and angular selection of the ESA.

Although not obvious from Table I. HYDRA consists of six pairs of anticollinear electrostatic analyzers of the classical 127° design mounted on the spinning space-

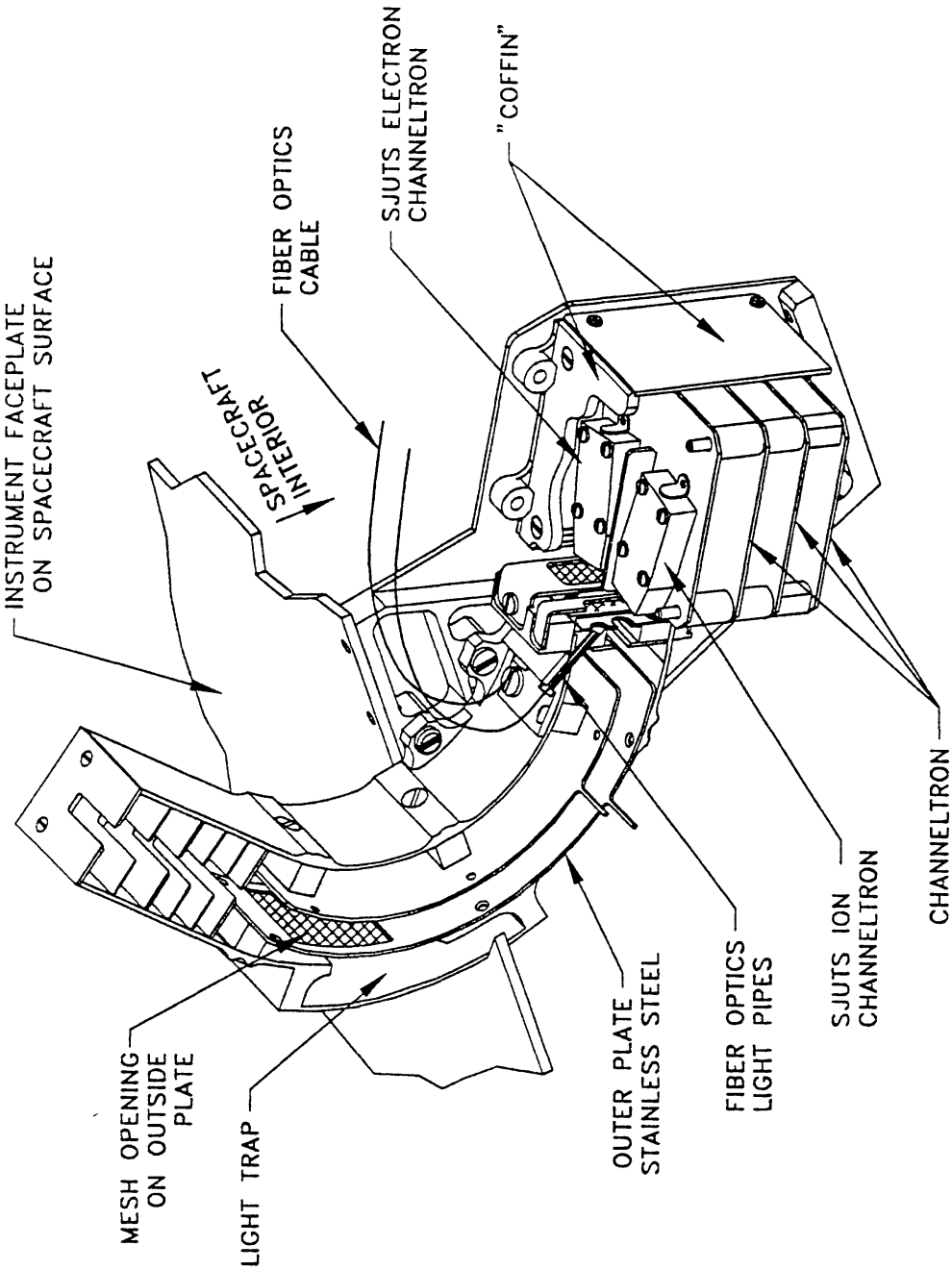


Fig. 5. DDEIS ESA Cutaway Isometric. Illustrates the shield configuration for the channeltrons. The thicker plate of the coffin has been shown in breakaway section to permit 'viewing' of the Sjut's channeltron deployment.

craft body. Adjacent odd and even numbered analyzers form pairs that permit nearly opposed samples of velocity space to be acquired simultaneously. The ESA's have narrow, symmetrical, balanced energy bandwidth of $\Delta E/E = 6\%$ determined by balanced deflection plates and slit determined solid angles. The narrow, mechanically defined fields of view are light trapped (cf., Figure 5) and have each been calibrated to have $8° \times 8°$ full widths at half maximum and $10° \times 10°$ full widths. Each 127° ESA has a directional geometry factor of $5.5 \times 10^{-4}$ cm$^2$ strd for protons and electrons. The slit determined geometrical properties of this analyzer can be determined from the planar conformal map of the cylindrical analyzer onto the plane of Figure 6. The conformal map preserves angles while allowing the optics of the curvilinear capacitor between the plates to be thought of as if it were a parallel plate capacitor.

The energy resolution of each 127° electrostatic analyzer assembly is $\simeq 6\%$ and has been measured for each analyzer-detector assembly after it is in flight configuration. The angular integrated energy transmission of the analyzer is illustrated in Figure 7(a). A small 3% contribution to the detector transmission comes from off angle transmission associated fringe fields accompanying the reductions of the mechanical size of the 12 ESA's to save weight. This off angle transmission is illustrated more clearly in the isometric angle-energy plot of Figure 7(b). 97% of the the analyzer's transmission is adequately characterized by the mean geometrical field of view of the channeltron associated with the principle peak of this figure. The steering voltages are *simultaneously* applied to all the DDEIS electrostatic analyzer plates in a given package by a dual range, digitally addressable, bipolar stepping power supply that produces staircase like voltage output waveforms. The energies that may be surveyed by the DDEIS and the PPA are indicated by the curves in Figure 9. Each DDEIS box has its own independent stepping supply that responds to DPU command. To change the levels the DPU sends identical step commands to both DDEIS units. The design of these supplies was a cooperative venture between Code 734 NASA-GSFC, the University of New Hampshire, and Vandiver Associates of Huntsville, Alabama. Although each channeltron retains its own bias voltage to count either electrons or ions, the energy per unit charge transmitted by the ESA plates may be switched by this stepping supply to allow either electrons or ions through the cylindrical gap to impinge on the channeltrons. Since the ion channeltron is biased at $-2000$ V with respect to the exit aperture of the analyzer, electrons are deflected from it, while ions are attracted. Electron 'splash' created by collected ions at the entrance of the ion channeltron are returned to the amplification process in the channeltron with a high voltage ('HV') mesh indicated in Figures 5 and 6 that is biased more negatively with respect to ground than the front end of the channeltron. The positive bias of the electron channeltron to ground obviates the need for a mesh for this reason; however, electrons made by any scattered UV photons within the deflection plates are substantially reduced by biasing the 'LV' mesh in Figure 6 at $-2$ V. This precaution implies that ambient electrons of energy lower than 2 eV cannot be directly sensed by the ESA's of

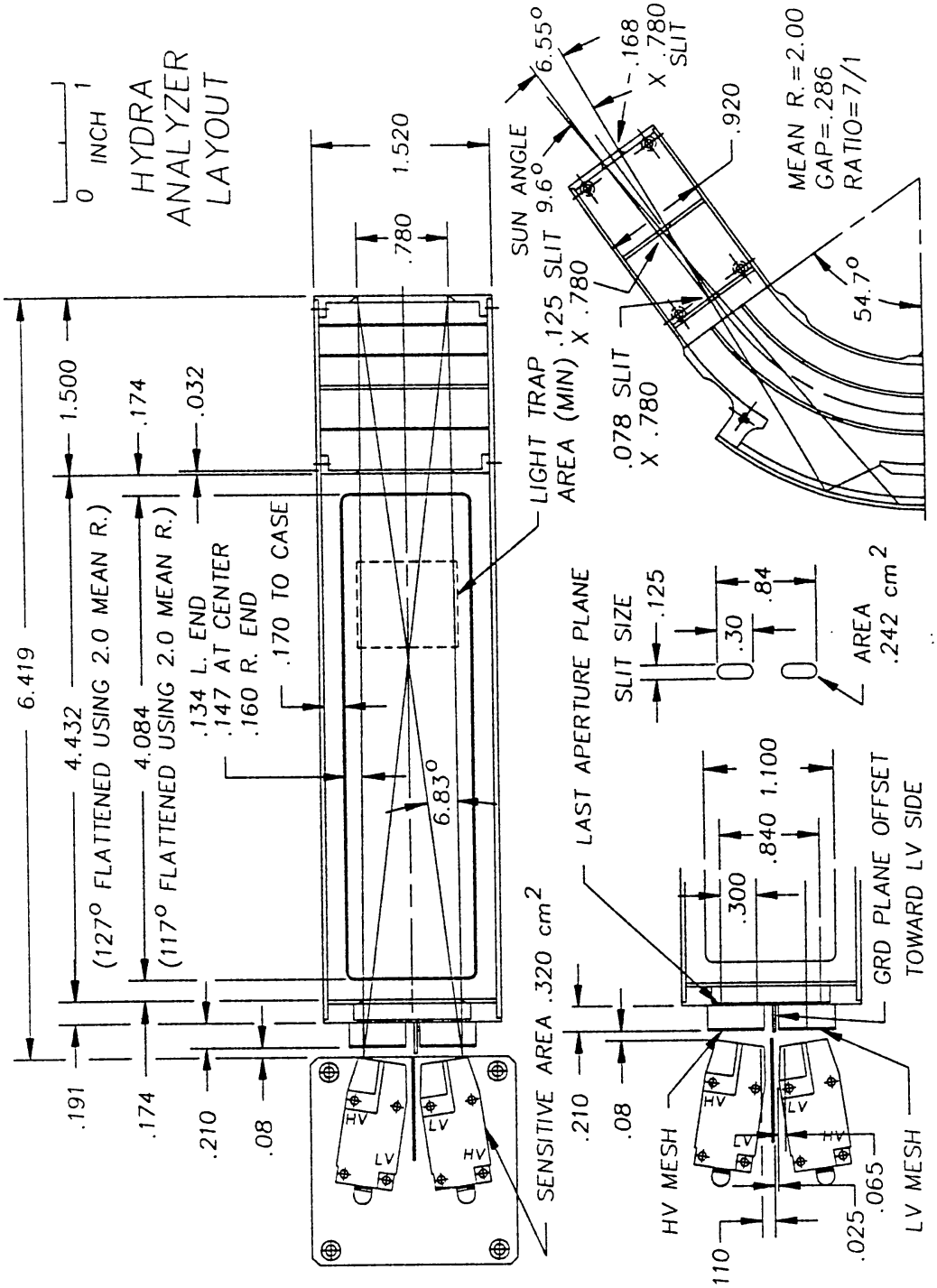


Fig. 6. DDEIS ESA Optics Ligth Trap and Channeltron Details. The right cylindrical section capacitor of the 127° analyzer is conformally mapped (preserving angles!) into the rectangular ray path diagram top center. Insert lower left illustrates the 'HV' and 'LV' meshes referred to in the text.

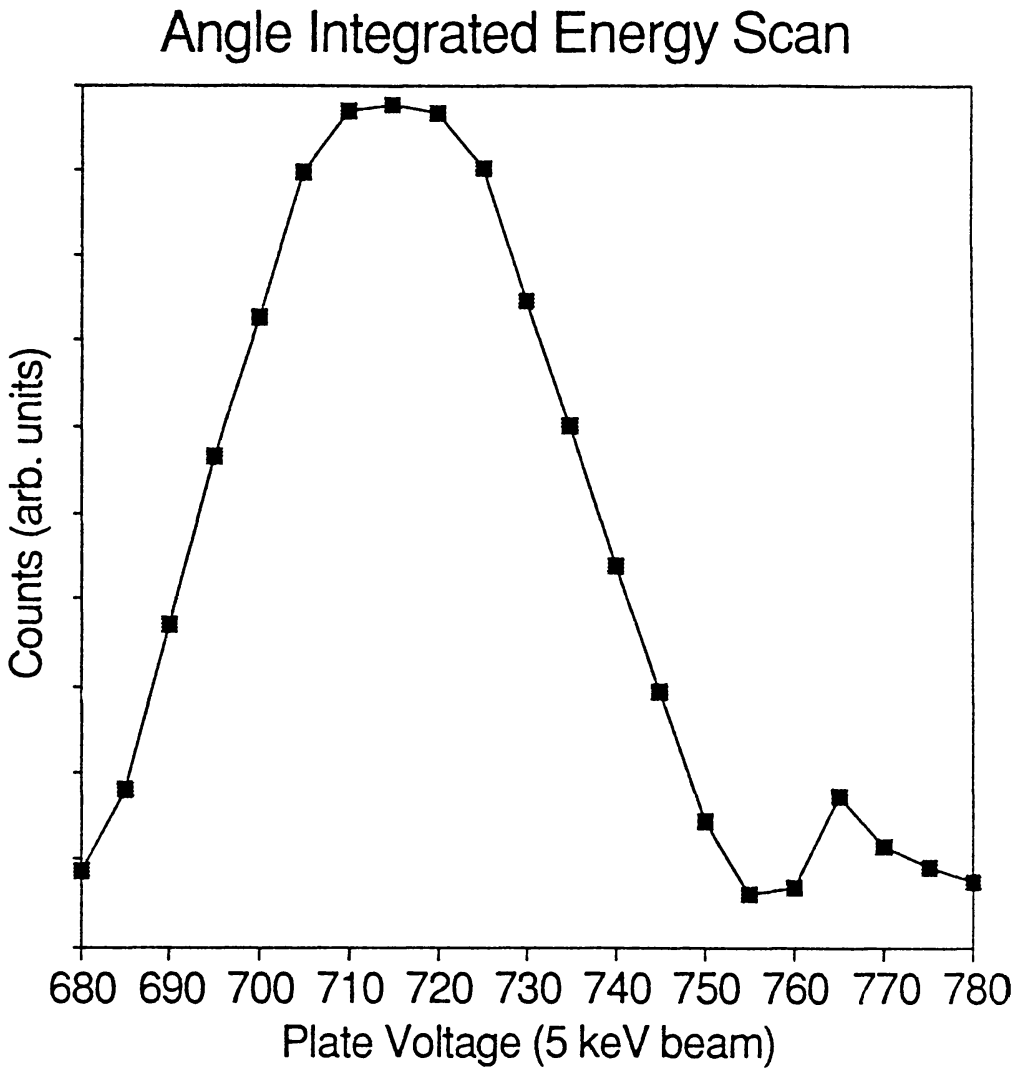


Fig. 7a. Angle Integrated Energy Ban Pass of DDEIS ESA.

the DDEIS unless the spacecraft floats positive with respect to plasma potential. The telemetry readout of the channeltron amplifiers is correlated with the polarity supplied by the stepping supplies: only the ion (electron) channeltron counter is queried when the ion (electron) polarity is applied to the stepping deflection supply.

The design of the power supply ensures that the magnitude of the opposite voltages applied to the ESA plates remain balanced even after radiation degradation of critical operational amplifiers. The geometry of the ESA and post fabrication calibration determines that the applied voltage on the plate is $\simeq 1/7.07$ the desired tuning energy of the analyzer. Since low energy auroral and ionospheric particles may be anticipated, selection of 2 eV particles is highly desirable. This implies symmetric 280 mV outputs in the lowest output range, while the highest plate voltage of 5 kev allows survey of particles with kinetic energy of 35 keV charge$^{-1}$. This wide dynamic range was obtained with a two range supply, the low range being

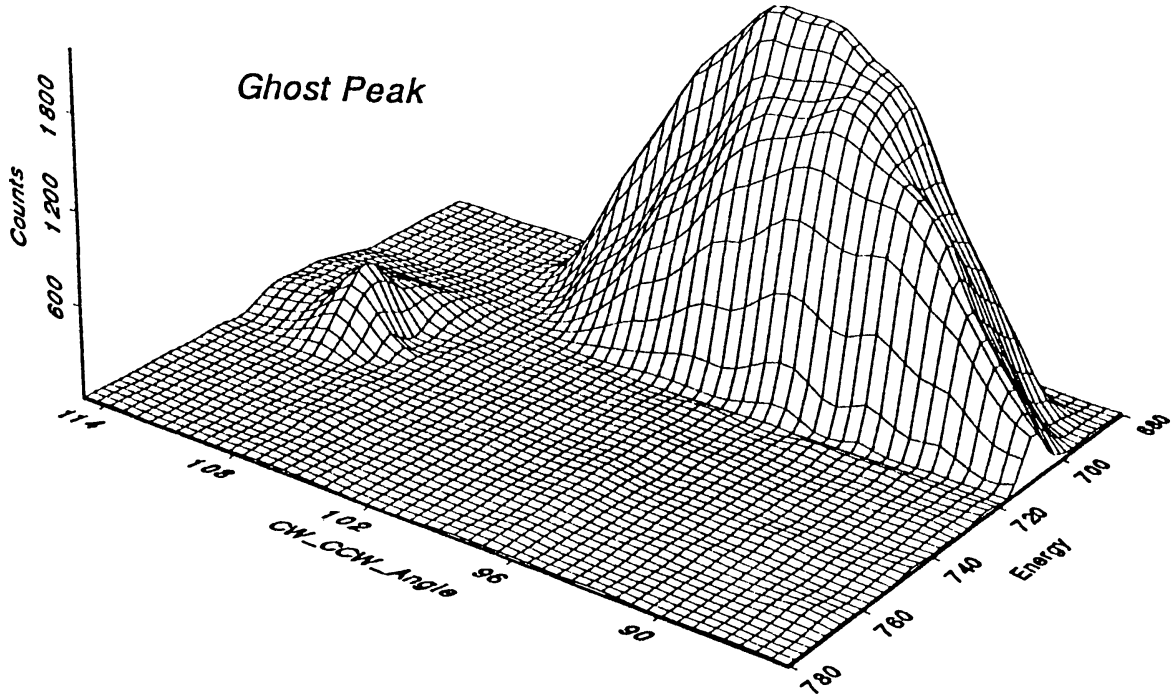


Fig. 7b. Energy-Angle Isometric Picture of Energy Ban-Pass.

supplied directly off of a transistor output and designed by Vandiver Associates in collaboration with the University of New Hampshire, while the upper range (of a more conventional design) was built by the Power Supply group of the NASA GSFC. The two parts of the supply are connected at the plates of the ESA and isolated from one another. By design the low and high voltage ranges of the supply have an overlap range for applied voltages to the plates between 5 eV and 10 eV. By requiring count rate profiles from the different stages of the supply to 'line-up' for plate potentials in this range, the limited range, but radiation immune solid state switched section can dynamically recalibrate inferences of low energy populations by the conventional supply (which has a wider dynamic range) that may degrade at low energies with radiation. The solid state switched supply is bipolar and has energy ranges below 2 eV, which can be used for the ion channeltron. The lowest transmitted energy for the ions is dictated by the lowest usable step of the supply which transmits $< 1$ e/$Z$ ions.

Together all of the ESA's of the DDEIS resolve electrons and ions in three dimensions with energy per unit charge between 2 eV and 35 keV with the very high time resolution (0.5 s) required to resolve the abrupt changes in configuration space of structured, subsonic distribution functions anticipated on the POLAR trajectory.

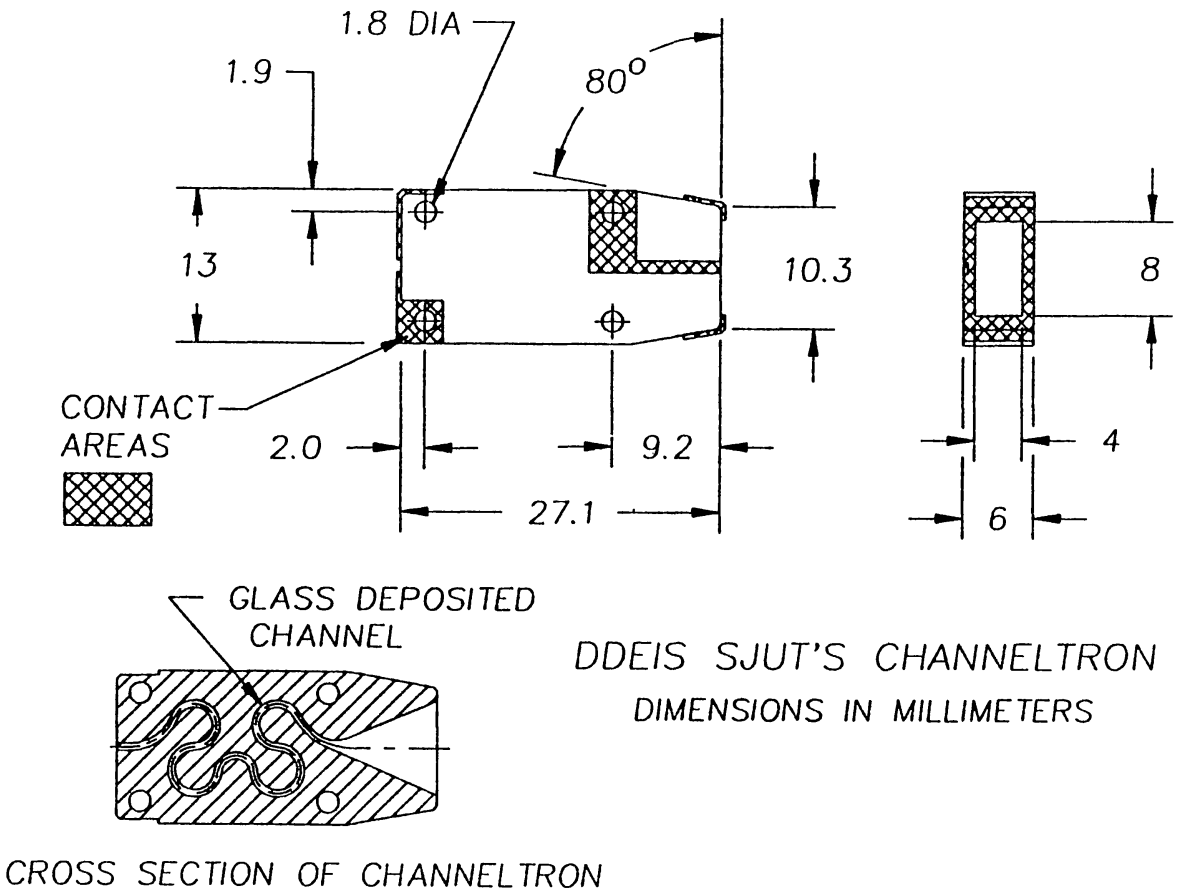


Fig. 8. Cross section of DDEIS Sjut's Channeltrons. Amplification occurs along glass deposited channel, starting in the rectangular horned mouth indicated by the triangle in the section drawing lower left and the end on view upper right.

## 2.2. Properties of the Parallel Plate Analyzers: PPA

In addition to the body mounted DDEIS optics, HYDRA, as originally proposed contained 2 additional pairs of narrow field aligned ESA's deployed on the two axis despun platform that was to have tracked the apparent variation of direction of the magnetic field in the rotating spacecraft's frame of reference. In the descoping activities prior to acquiring 'new start' status this despun platform was deleted. As in mythology HYDRA was thus deprived of 4 of its originally proposed ESA 'heads'. The Parallel Plate Analyzer (PPA) was designed in response to the 'technology enhancements' that were considered when the GGS program gained its new start status. The objective of the PPA design was to recover high angular resolution measurements in the loss and source cones along the magnetic field from a body mounted instrument. Telemetry requirements soon made it clear that this device was best suited for electrons rather than ions, since the ions have detectable cross field drifts that require a full three dimensional phase space to be packed into the telemetry rather than just pitch angle and energy. The classical PPA analyzer

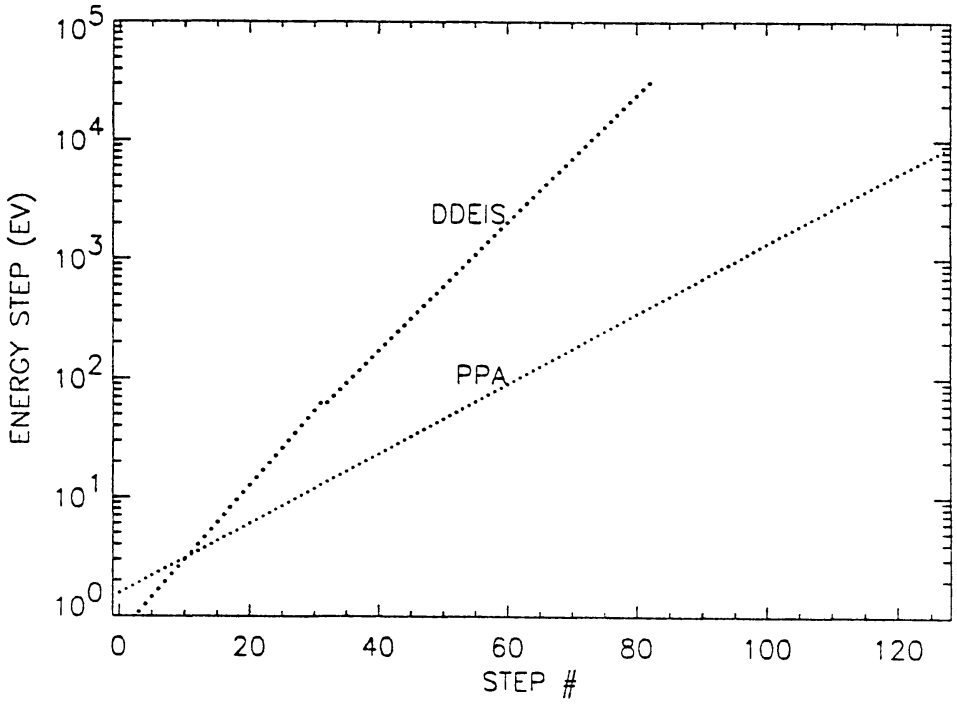


Fig. 9. Tunable Energies for DDEIS and PPA stepping supplies. The supplies are digitally addressable. There are some constraints on the rapidity with which two widely different energies can be sought in succession that limit otherwise random sequences of energies to be planned.

(Green and Proca, 1970) was modified to incorporate a light trap (Herrerro, 1991) so that particle 'images' of a conical field of view of half angle 15° might be made in the presence of scattered sunlight on a two-dimensional, position sensitive. coded, microchannelplate detector called a *codacon*. This electro-optical device is illustrated in schematic breakaway isometric section in Figure 10. Negative voltages can be applied to the three plates above the grounded plate with the pinhole and semi-circular exit ring. The modified parallel plate ESA portion with light trap selects the electrons by energy and direction and turns them nearly 90° to impinge on the micro-channelplate stack with a mean trajectory indicated by the dashed curve. Electrons that approach the pinhole at clock and cone angles to the mean trajectory are dispersed in two dimensions onto the the codacon's plane of sensitivity. The codicon micro-channel plate stack (located at and below the plane of the cross within the circular cutout of the codacon electronic box) was constructed at LASP, University of Colorado at Boulder under the direction of George Lawrence. By design the codacon and electrons gives a 10-bit address that defines where the counted particle has struck the plane of the codacon.

The main difference from the classical PPA design is the large gaps in the deflection plates. These holes permit the light trap which gives the device its reduced UV sensitivity. This gap is so large behind the aperture that traditional mesh methods for maintaining planar equipotentials witin the plates could not be tolerated for fear of the enhanced sunlight scattering they would produce. The fringe fields around the gap in the plates creates a new form of lensing as compared

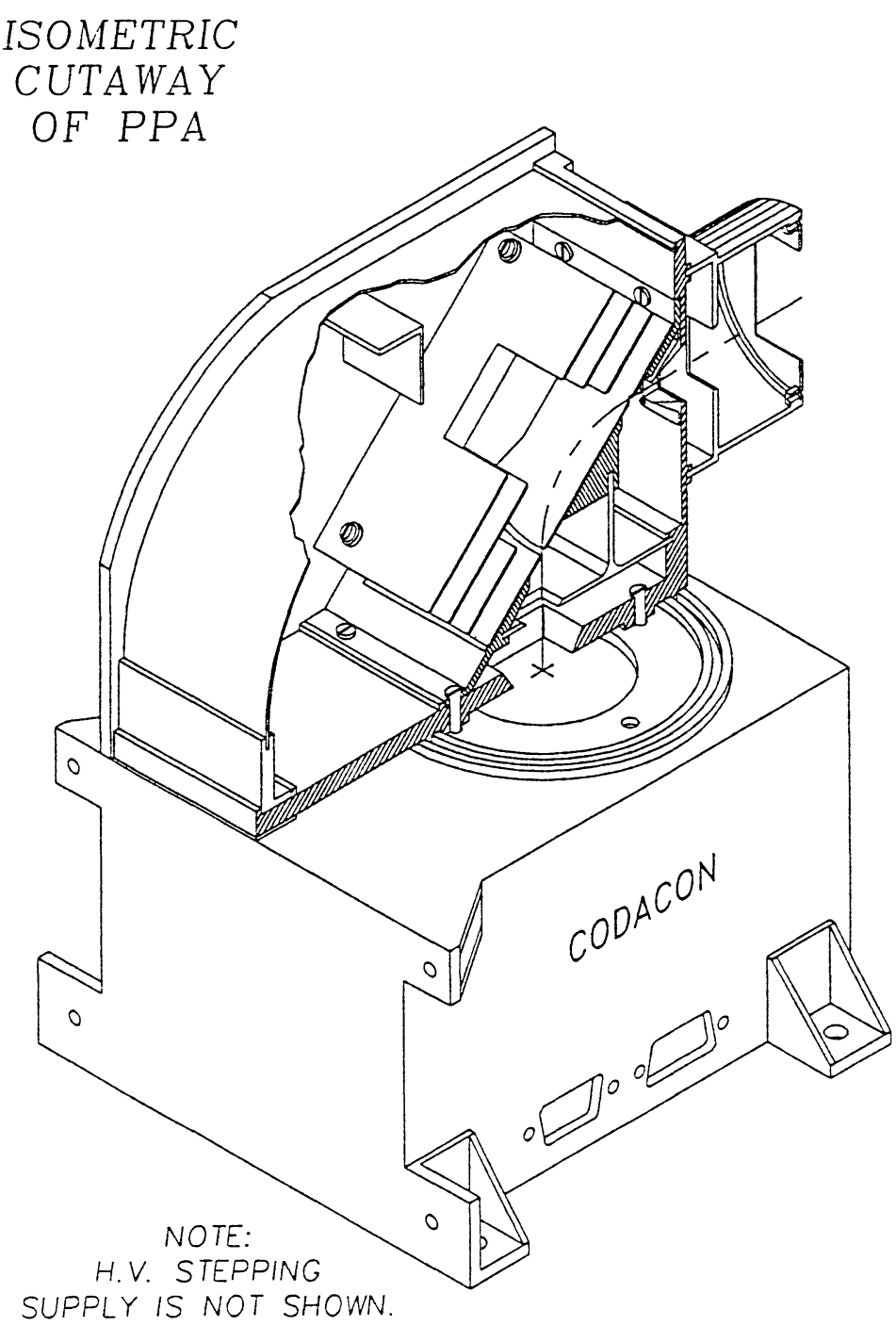


Fig. 10. PPA Mechanical Arrangement in Breakaway Section. The four 'steering' plates inclined at approximately 45° to the entrance trajectory are the remains of the traditional parallel plate ESA. The 'gaps' in the plates allow *photons* to enter the rear volume which performs as a light trap discussed in the text. High voltage stepping supply for the PPA bolts to the four holes on the end of the codacon box. The microchannelplate stack of the codacon are located in a plane through the + parallel to the interface plate between the optics and codacon proper.

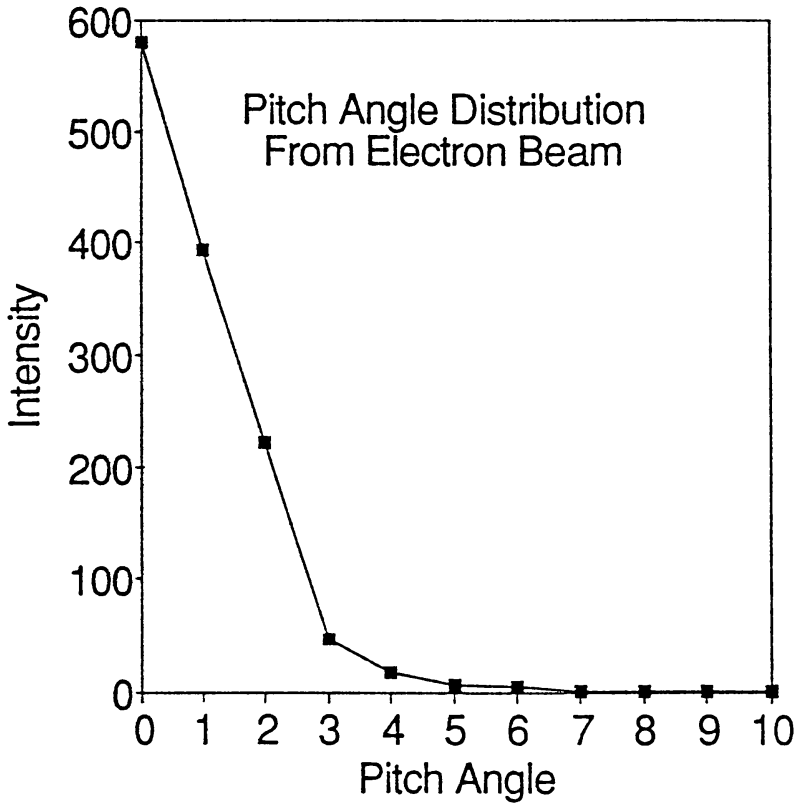


Fig. 11. Experimental Demonstration of Pixel Resolution on the PPA. Data were taken by pointing an electron beam directly at an individual pixel and setting the magnetic field vector (input to the sorter board) to that pixel. Data are the averages taken over several runs across the detector with each run incrementing $\phi$ by 2°. Data have been normalized to the solid angle seen by each pitch angle, the effect summarized in Figure 12.

with the usual PPA analyzer. The full width angular resolution of a 'pixel' on the codacon as measured is approximately 1.5° (cf., Figure 11, below) compared to the 10° conical field of view of the electrostatic analyzers in the DDEIS discussed above. After energy selection in the parallel plates, an electron strikes the codacon somewhere on a 32x32 position sensitive array, where a 10 bit position sensitive address is electronically generated. This information, together with the corrected on board magnetic field data are fed into the sorter board of the DPU which determines the corresponding pitch-angle register to increment so as to record the sorted count (Keller *et al.*, 1991). This approach represents a tremendous telemetry compression scheme over the direct transmission of the individually counted particles with their geometry. The 256 pitch-angle registers can be reprogrammed to subtend a variety of pitch-angle intervals as needed. The optical angular resolution of the pixels is about 1.5° as illustrated Figure 11. This sorting process is accomplished without difficulty for plate integrated counting rates in the Mhz range. In this way the 4 ESA 'heads' that were lost by the budgetary action of deleting the despun platform, are now replaced with 1024 ($32 \times 32$) pixels 'heads' in parallel with the story of Greek mythology.

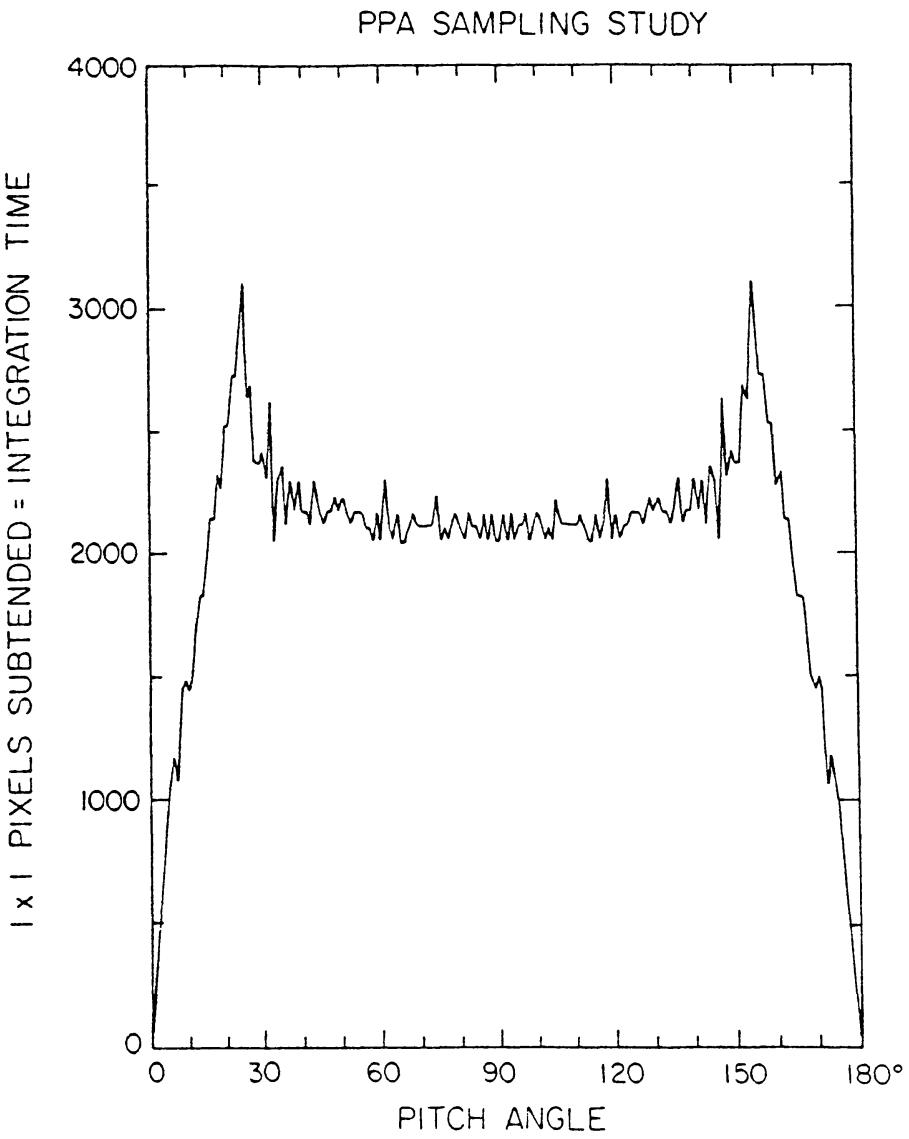


Fig. 12. Geometric Enhancement Factor of the PPA with Pitch Angle if $B$ is located in the spin plane as would ocur with the nominal Polar orbit and attitude.

The wide field of view of the PPA invariably includes the sun once per PPA box, per revolution. The microchannel plates of the CODACON are UV sensitive and scattered UV could represent a significant omni-directional background. UV effects for the PPA as built have been modeled, measured and shown to be sufficiently surpressed at the codacon image plane as discussed extensively by Herrero (1991).

Each of the PPA units has a field of view in velocity space that is the mirror image of the other in the spacecraft coordinate system. Each PPA box contains its own unipolar (−) deflection power supply. The supply only selects electrons with kinetic energy between $\simeq$ 100 eV and 10 keV with $\simeq$ 20% energy resolution. These stepping supplies are simultaneously commanded by the DPU, but on a time line that is independent from that of the DDEIS. In general the tuned energy of the

PPA's will not change faster than twice per spacecraft revolution. There are several voltage steps in the auroral bearn energy range where the PPA transmitted energy and that of the DDEIS system can be made to be the same for intracalibration. The transmitted energy per unit charge steps of the power supplies for the DDEIS and the PPA are illustrated in Figure 9. The geometric factor per pixel is $1.7 \times 10^{-3} E/1$ keV cm$^2$ strd. The anticipated amplification of the per pixel geometric factor with pitch angle per spin is illustrated in Figure 12 under the assumption that the magnetic field lies in the spin plane of the spacecraft. Geometric factors of the order $1.7E$/kEV cm$^2$ strd pixel$^{-1}$ are achieved by the PPA concept.

As the spacecraft rotates, PPA count data from both PPA boxes is sorted continuously. As the 30° full width aperture of the PPA sweeps in S/C azimuth, different pixels subtend different pitch angles, because the magnetic field and the pixels will both have changed their relative locations between successive counts. Data will be collected simultaneously on both PPA's through the same sorter electronics at a common energy for $\frac{1}{2}$ spin of the spacecraft. In this time with high probability approximately 30 different pixels will 'see' the singular directions near a given pole of the pitch-angle space, and the opposing PPA will have provide the same information for pitch angles 180° removed. However, as the pitch angle sampled moves away from the poles, upwards of 3000 samples can be integrated to delineate the pitch-angle distribution for pitch angles removed from $\pm\hat{\mathbf{B}}$. The PPA delivers a full pitch-angle sample at all pitch angles for a given energy twice per spacecraft rotation. By special command either PPA unit can be the sole input to the sorter board. Another special command allows the raw count rate information from either or both PPA sensors to be multiplexed directly into the telemetry to verify the sorting algorithm.

Because the PPA concept uses azimuthal motion of the $S/C$ to enhance angular resolution, the time resolution of the PPA is correspondingly reduced. Because the singular direction of the magnetic field is only traversed once per half spin. an angular survey requiring a view along the singular field direction cannot be acquired faster than $\simeq$ 3 s which is half the spin period. To get a full energy range, high angular resolution pitch-angle picture of the distribution function from the PPA will require multiple spins. With the onboard DPU software we have foreseen that the coarse angular resolution DDEIS survey may at high time resolution 'inform' the PPA of the interesting regime to concentrate its energy sweeps. Our updated software algorithms will allow this type of interplay to make optimal use of the PPA to enhance the overall angular resolution of the distribution in those energy regimes where the DDEIS is indicating strong gradients in speed or in angle.

The central assumption of the PPA system is that the distribution function is time stationary in the magnetic field's frame of reference and hence does not have an observable cross field convection. Thus, when the more rapid DDEIS samples indicate that $f(\mathbf{v}, t)$ is relatively steady, the high angular resolution distribution function determined by the PPA can be reduced down to the DDEIS sampling frequency without fear of time aliasing. The PPA high angular resolution 'picture'

of $f(\mathbf{v})$ can then be degraded to compare with the low resolution pitch-angle map made with the DDEIS alone. In this way the PPA and DDEIS can be relatively calibrated in flight. Since the DDEIS absolute calibration is tied to the local determinations of the plasma density through the PWI determinations of the plasma frequency, the entire HYDRA system is, by transitivity, absolutely calibratable in flight.

The ground analysis of the PPA's binned count distribution requires the knowledge of the polar angles of the magnetic field used on board in the sorting process. The high resolution polar angles of $\mathbf{B}$ used by the PPA sorter are telemetered to the ground *within* HYDRA's telemetry for calculation of the normalizing probability that a given pitch-angle interval was possibly seen during the data acquisition interval that corresponds to the binned data. An example of this type of pitch-angle reconstruction is illustrated in the key parameter section below.

### 2.3. UV INTRACALIBRATION SYSTEM

Central to the successful achievement of our scientific objectives is the intracalibration of the separate channeltron assemblies which subtend each of the cylindrical electrostatic analyzers in the DDEIS. There are several approaches to this problem. Internal consistency of the pitch-angle distribution in strong magnetic fields can be enforced by requiring the *invariance* of the pitch-angle variation of *separate* analyzers at the same energy. To be defensible this approach requires a strong field with no substantial cross field convection present. To assist this approach the HYDRA investigation also contains an Ultraviolet Lamp calibrator source manufactured by Resonance Ltd of Canada illustrated in Figure 13, which is attached to the DPU box and facilitates a relative calibration between ESA's. When powered this lamp source provides a copious source of UV photons to a pair of matched length UV fiber optic cables providing a common UV intensity source to the two separated boxes of the DDEIS on opposite sides of the spacecraft and on different instrument shelves. The transmissivity of the UV light pipes will degrade with radiation dose. By using matched length lines we have attempted to obtain a matched degradation of the transmissivity of the UV to the DDEIS boxes. At each DDEIS box a UV fiber optic connector splits the single light pipe from the calibrator into twelve light pipe connectors which fan out to the rear of each electrostatic analyzer where each is aimed to illuminate both channeltrons of each specific analyzer. Since the channeltrons are activated by UV photons as well as by particles, determinations of the relative counting rates of the analyzers to the common source will help to establish the relative degradations of the channeltrons with use. Degradation of the channeltron gain can be compensated on command by increasing the bias voltage across the channeltrons. On board measurements of the channeltron pulse height distribution will also be multiplexed into the telemetry stream to guide the appropriate choice of the voltage and to allow routine confirmation that the channeltrons remain 'saturated'. The UV calibrator's power is directly controlled by

the DPU; it will be off when particle measurements are being performed by the ESA's. During the UV calibration the ESA deflection voltages will be parked at a voltage where the transmitted flux is lowest; science data collection is interrupted by this infrequent but necessary on orbit calibration activity.

### 2.4. THE DATA PROCESSING UNIT AND ITS PROPERTIES: DPU

The Data Processing Unit (DPU) is a derivative of the DPU developed and built by the University of New Hampshire for the SWE instrument on GGS/Wind as described by Ogilvie et al, 1994. All the internal boards of SWE's DPU design are identical to four of the boards in the HYDRA DPU. These boards consist of a processor, an interface to the DDEIS's, an interface to the spacecraft, and a storage memory-power supply board. The PPA sorter subsystem is unique to HYDRA and requires an additional board in the DPU to perform in flight pitch-angle sorting necessitated by telemetry constraints. A *sorter* board was added to the HYDRA DPU to perform a hardware look-up table of the scalar dot product of an incoming particle's velocity with the ambient magnetic field. This was possible by exploiting the many trigonometric simplifications made possible by the symmetries of the detector's deployment. The implementation of the sorter board is described in Keller *et al.* (1991). The DPU is packaged together with the attached UV calibrator discussed previously (illustrated in Figure 1). The typical power consumption of the DPU alone is 2.2 W.

In addition to the unique sorter board, the HYDRA DPU has Polar unique *intra-instrument* communications schematically indicated in Figure 2 between HYDRA and the magnetometer experiment, MFI (described by Russell *et al.*, 1994) the electric field instrument, EFI (described by Harvey *et al.*, 1994) and the low energy ion detector, TIDE (described by Moore *et al.*, 1994). The DPU receives raw magnetic field data at an onboard rate of 100 vectors per second, corrects it for zeros and offsets, converts its direction to the equivalent spacecraft polar angles, and filters it as appropriate for use in the sorter board. The interconnects with EFI and TIDE are used as signals of burst mode acquisition for coordinated high data rate collection. In the case of EFI, the protocol allows either EFI or HYDRA to alert one another of its change of status to the burst mode; the receiving instrument may or may not choose to respond in kind. The interconnect with TIDE only allows TIDE to 'listen' to HYDRA's burst mode status so that it may coordinate its data acquisition if desired.

The DPU is powered by a Sandia SA3300 CPU and SA3304 timing control unit which is a radiation hardened version of the National Semiconductor's 32C016 microprocessor. As this device is extremely fast and fiexible, considerable mode adaptation is foreseen with this instrument as we learn its on orbit capabilities and those of the detectors. The processor also contains 8K bytes of fuselink PROM, 32K bytes of RAM and 128 K bytes of EEPROM. The PROM contains code for system testing, default system configuration, reading and interpreting commands,

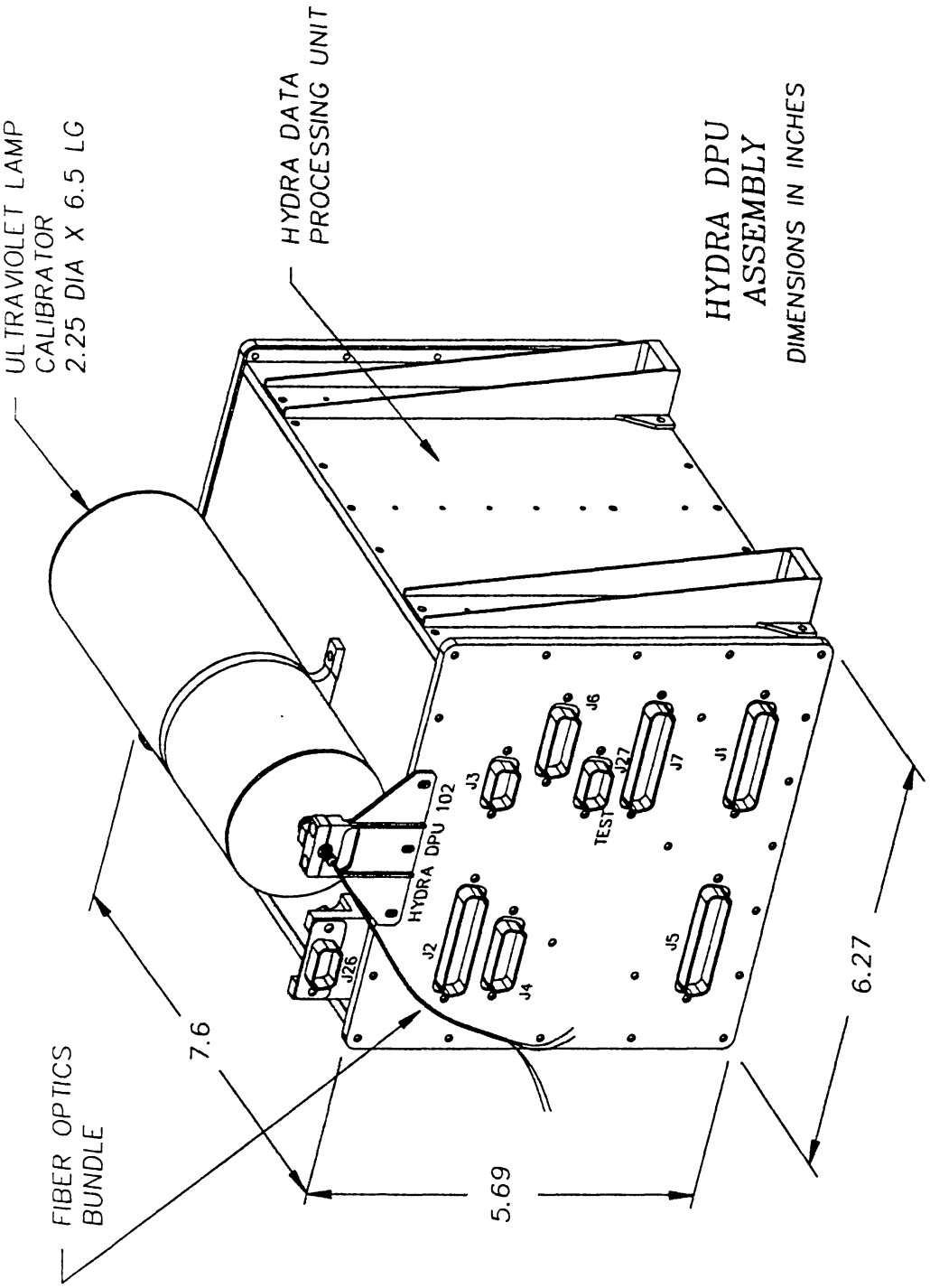


Fig. 13. Isometric of DPU and UV Calibrator with Fiber Optics Bundle.

a boot mode of operation, and two fault isolation modes of operation. Additional code can be uplinked in flight and stored in EEPROM. Additional circuitry in the processor system provides a hardware watchdog timer, processor reset and EEPROM write protects in case of software upset .

The DPU interface to the DDEIS *intra-instrument interface card* uses a 1 MHz serial link to send commands for system configuration, relay actuation, high voltage control, pulsing charge amplifiers, and charge amplification pulse height analysis. The system also sends a reply for housekeeping monitoring and data transmission checking. The DPU interface to the spacecraft receives telemetry timing, spin rate data, absolute time data, telecommands and transmits telemetery data. A memory array of 1.5 Mbytes of non-radiation hardened static RAM is provided for fast event data storage for later telemetry transmission. Since this soft RAM memory may fail sometime during the mission, power and bus isolation protects the rest of the DPU upon failure; upon soft RAM failure this system also switches the soft RAM's ±28 V power to the DDEIS for further distribution to the HYDRA packages on the spacecraft perimeter. Housekeeping monitors track currents for each subsystem and DPU internal voltages.

In the science software, an architecture built around 'descriptors' has been designed by UCSD in collaboration with UNH and other co-investigators. Descriptors allow varying combinations of energy sweeps, dwells and frequency of electron or ion data acquisition, or loops thereof to be selected with a limited amount of commanding. A telemetry synchronous *boot mode* is incorporated into the flight memory that can return basic data for a successful mission; the telemetry and sampling of the detectors are not spin synchronous in this mode. This boot mode is not the anticipated mode of routine deployment of the instrument. A Sun-synchronous mode will be the routine mode of the instrument. The time resolution and the discussions below for the various instruments are based on a nominal energy sweep rate of approximately 0.5 s which characterize the boot mode. The Sun-synchronous modes have sweep rates that are minimally smaller than this, given the lack of commensurability of the spin period and the telemetry major frame structure. A Sun-synchronous data acqusition requires more code space than could be stored in our 'boot', or default, mode. Even in the boot mode ions and electrons may be interleaved or not, or entire periods of time dedicated to one or the other sign of charged species or at a fixed particle energy to monitor time variations. *It is anticipated that the routine mode of the DDEIS will he comprised of interleaved electron and ion sweeps during which all ESA's will observe the same species and record counts at the same energy at the same time.*

## 3. Data Collection Strategy

The primary observable for this instrument is the distribution function. In this section we visually display the practical consequences of our detector properties

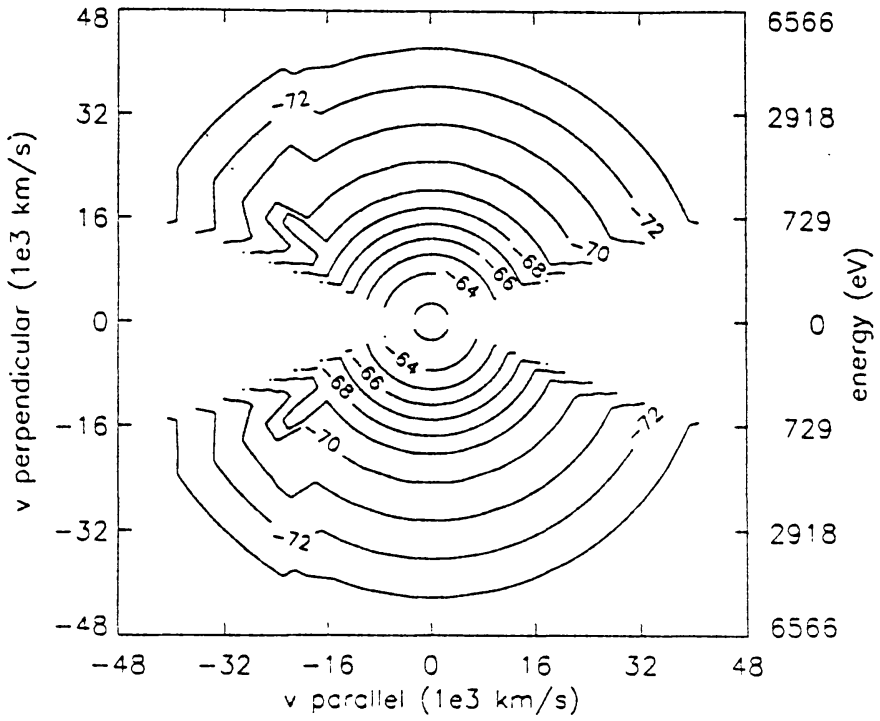


Fig. 14. Mirroring distribution upstream at ISEE VES resolution.

and geometry. For convenience we assume a model distribution with substantial angular structure induced by field aligned potentials and mirroring to compare the ISEE/VES viewing resolution with that of the DDEIS at comparable time resolution, while permitting an appraisal of the ultimate angular resolution possible when time stationary permits a full PPA energy sweep to be accomplished. The various models and observations associated with parallel electric fields in the strong mirror magnetic field configuration suggest that the empirical determinations of the boundaries of phase space separatrices may be the best way to diagnose the presence of parallel electric fields that are often too weak to be detected by traditional DC field methods (Whipple, 1978; Mizera and Fennell, 1977).

With HYDRA's 12 rather than 6 ESA's of the VES the 'fuzzy' signatures of the mirrored distributions in Figure 14 from ISEE which are quantitatively sharpened Figure 15: HYDRA, a comparison performed with ISEE's fastest time resolution of 6 s.

When time stationarity warrants, additional angular coverage can be included to further enhance the angular details of the same underlying distribution as illustrated in Figure 16 with a time resolution of 9 s which includes 18 energy sweeps on the DDEIS. During this time loss or source cone information at a given PPA energy may be determined twice per spin. Within the time interval of the DDEIS sarnples of Figure 16, four complete PPA sweeps are completely in the telemetry (at this time resolution the PPA telemetry and DDEIS telemetry are not quite in phase).

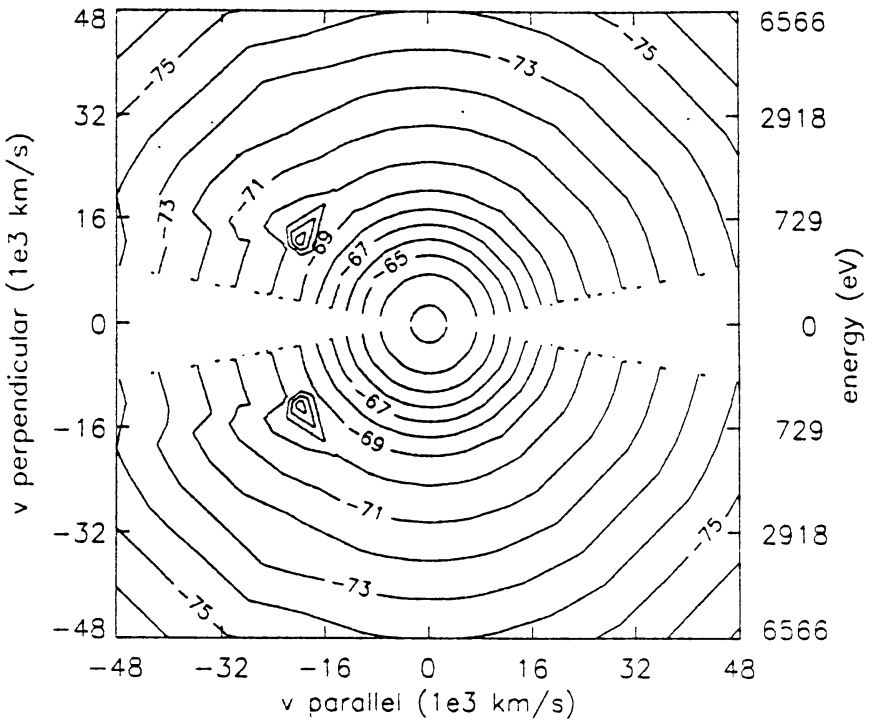


Fig. 15. POLAR DDEIS (only) 'view' of same distribution as in 14. No PPA samples are included. Time aliasing of this sample and that of Figure 14 are the same, 6 s.

Using four energy dwells of 0.5 s each the PPA pitch-angle resoultion further sharpens the underlying picture as illustrated here.

In another mode the microprocessor may command the high voltage stepping supplies to the DDEIS to 'dwell' at the same energy while still reading out the DDEIS registers at regular intervals. In this way a detailed picture of possible gyro-mechanical free energy at a given energy can be inventoried, especially from the DDEIS ion data. The evolution of such a surface could be followed with a frame rate of 30 ms.

Every 3 s a PPA energy sweep passes through the singular magnetic field direction and a determination can be made if there is loss or source cone 'activity' near the field direction. This determination is made at fixed electron energy by assessing the departure of the flux pattern near the 0 pitch-angle buckets versus that expected for the intercepted field geometry. An example of the PPA pitch-angle distribution when an isotropic pitch-angle distribution is present is illustrated in Figure 12 where a magnetic field in the spin equator of the spacecraft has been assumed. The ordinate of this figure is the number of times a $1° \times 1°$ pixel at the codacon plate *contributes*, other things being equal, to the accumulation of counts in the given pitch-angle bucket. Predictions of an adjusted scalar multiple of the pattern like that in Figure 12 based on the actual field directions used during data collection will be differenced from the observed variation. Consistent trends away from this pattern can be inventoried for optimizing the PPA energy sweeps

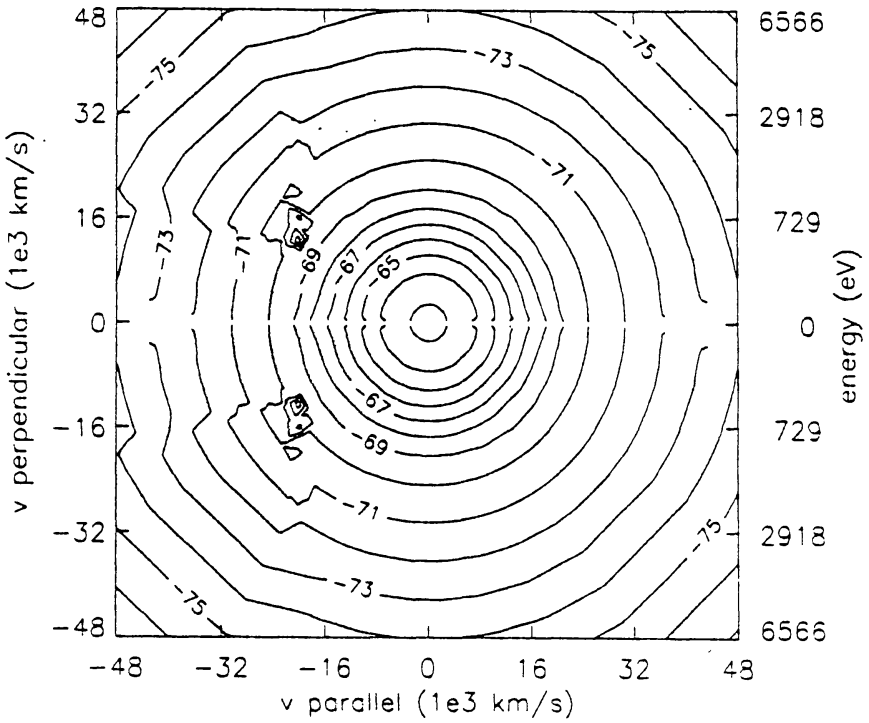


Fig. 16. POLAR HYDRA (including PPA) 'reconstruction' of $f(\mathbf{v})$ at a time resolution of $\simeq$ 9 s. Notice the imporved clarity of the the mirrored population. It is the defintion of this separatrix with energy that allows particle detectors to infer non-locally parallel electrical potential drops.

which are independent of those on the DDEIS to maximize the HYDRA science return. The key parameter algorithm will use the average magnetic field in the key parameter file rather that the computer intensive proces of constructing the analogue of Figure 12. The subsequent high interest intervals can be processed by first constructing the analogue of Figure 12 for the data interval and then dividing the observed pitch-angle rate distribution by the relative number of times predicted in Figure 12 that particles could be seen by any part of the PPA codacon sensor.

To maximize the scientific return of the acquired science from the GGS 'store and dump' spacecraft, onboard coordination of two types has been implemented between HYDRA and I) MFI, the magnetometer for high rate field data and II) EFI and TIDE for coordination purposes in data acquisition. HYDRA 'listens' only to the magnetometer information which the sorter board uses for placing counts into pitch angle buckets as a data compression scheme. The second group of intra-instrument connections are designed to coordinate high time resolution data acquisition that represents a reprioritizing of our use of telemetry. With the electric field investigation (EFI) HYDRA has a two way communication allowing *either* instrument to inform the other that they are in 'burst mode' prepared state. The TIDE link is 'send only' for HYDRA and listen only for TIDE. This line informs TIDE of HYDRA's burst mode status. HYDRA *cannot* anticipate a unilateral burst mode acqusition from the TIDE experiment.

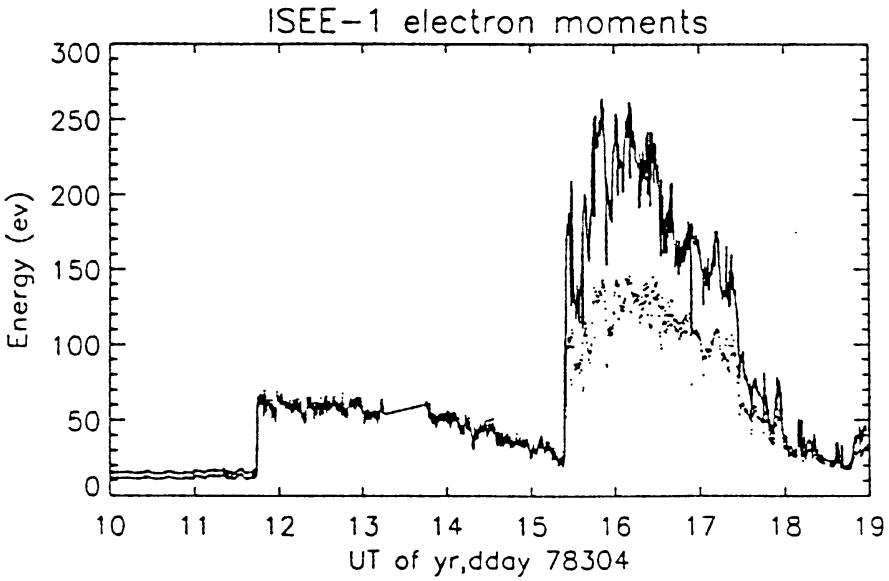


Fig. 17. Comparison of Detailed Temperature fluid parameter as $\frac{1}{3}$ the $Tr$ of the temperature tensor vs the key parameter that is closely related to it. Note that the key parameter data clearly identifies the rmajor boundaries as does the more computationally intensive proper $T$.

The *burst* signals between HYDRA, EFI, and TIDE were tested during the POLAR last comprehensive performance test. The EFI signal was determined to be active *low*, that is the EFI signal to HYDRA and TIDE is normally *high* and transitions *low* when EFI is storing burst data. The HYDRA signal to EFI and TIDE is active *high*, that is, it is normally *low* with a transition to high when HYDRA is storing burst data.

HYDRA will utilize the *burst* signals as follows: HYDRA BURST MODE consists of three phases: Pre-burst, Rapid Store, and Post Burst. When an event requiring burst mode is anticipated, HYDRA will enter Pre-burst Mode. In this mode, high time resolution data is streamed through a RAM buffer. The HYDRA burst signal remains *low* during Pre-burst mode. When a trigger occurs (see below for trigger options), HYDRA will enter Rapid Store mode and set the HYDRA burst signal high. During rapid store mode, a predetermined amount of data surrounding the trigger event is stored in RAM. The stored data will include data collected prior to and following the trigger event. At the end of the Rapid Store interval, HYDRA will set the burst signal *low*. HYDRA will then enter Post-Burst Mode during which the stored data may be read out. The trigger mechanism for HYDRA can be from one of three sources: direct command, internal algorithm based on data or EFI burst signal. Each of these mechanisms may be independently enabled.

## 4. Data Products

### 4.1. KEY PARAMETERS

We plan to use the key parameters of HYDRA and those of other instruments as originally intended: to delineate interesting events for higher order more quanitative analysis. We do not propose to complicate the key parameters by reporting 'odd' moments of the subsonic distributions nor the absolute density. In the first case the odd moments require considerable care and study before they can be validated, a concept alien to that of the key parameters. The absolute density as determined by a subsonic detector is exponentially dependent on the correct floating potential assignment. This is also an art form.

Low-energy plasma data reduction progrars are notoriously difficult to automate, particularly in the presence of the inflight, and, yet to be determined photoelectron contamination. This task is complicated by the need for a routine and accurate determination of the spacecraft floating potential variability in response to varying external conditions. In view of this circumstance the key pararneter philosophy of the HYDRA team is to produce quantities that are relatively immune to these problems.

As key parameters HYDRA's CDHF code will routinely produce two different estimates of the mean energy of the sampled electrons and ions. It will also provide an index that says a 'beam' or 'void' has been detected in the loss/source cone region, whether it is a loss or source cone or both, and at what energy it was inferred to be present. Almost all the visual products used in this instrument description are produced at a level of processing that is above that of key parameters. To illustrate the key pararneters diagnostic value of regime we have used our key parameter approach to process an orbit of ISEE data as illustrated in Figure 17. In this figure we contrast the temperature, T. as the one-third the trace of the temperature tensor **T**,

$$T \equiv tr\mathbf{T}/3\,,$$

versus a mean energy $\langle E\rangle$, where $\langle E\rangle_k$ is determined for each species without attempting the full up three dimensional moment analysis or disentanglement of other ions:

$$\langle E\rangle_k \equiv \frac{2}{3}\frac{\Sigma_{s,i,j} C^k_{sij} E^{k\,1/2}_j}{\Sigma_{s,i,j} C^k_{sij} E^{k-1/2}_j}$$

In the above expression $C^k_{sij}$ is the observed counts per unit time for the $k$th sign of charge species, in the $s$th energy, in the $i$th detector, on the $j$th energy level, $E^k_j$. The solid curve depicts $T$ from the moments, including correction for spacecraft charging and photo-electrons for one half an ISEE orbit, while the dots indicate

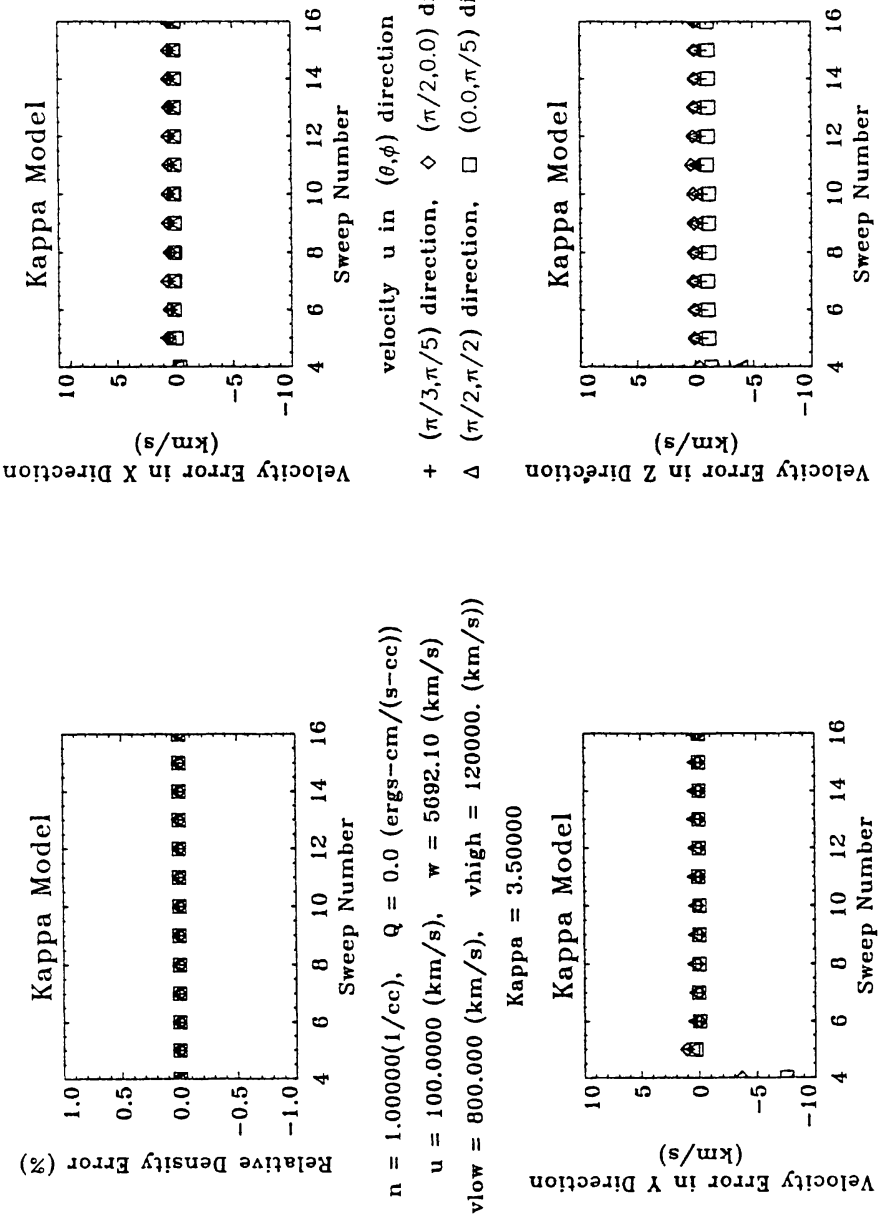


Fig. 18a.

Fig. 18a–c. Illustration of high precision moment recovery on model problems with proposed HYDRA sampling strategies and energy sweep rates for representative, flowing, ultra sub-sonic $\kappa$ distribution. Model parameters $n = 1/cc$. $U = 100$ km s$^{-1}$, $T \simeq 100$ eV, $q_{\parallel} = 0$. Of importance is the comparable and high precision of the vectorial and tensorial components.

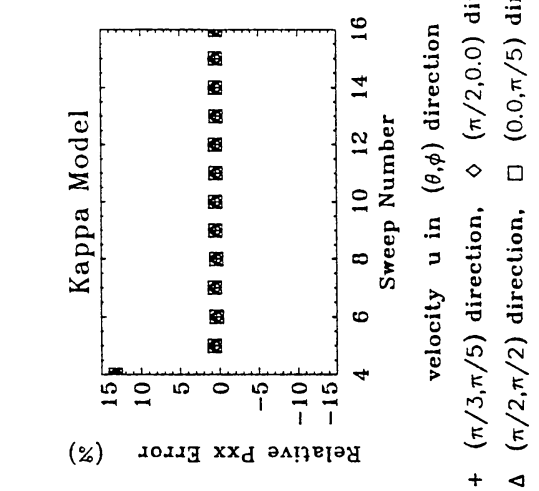


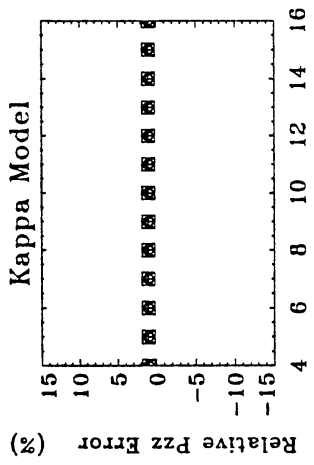


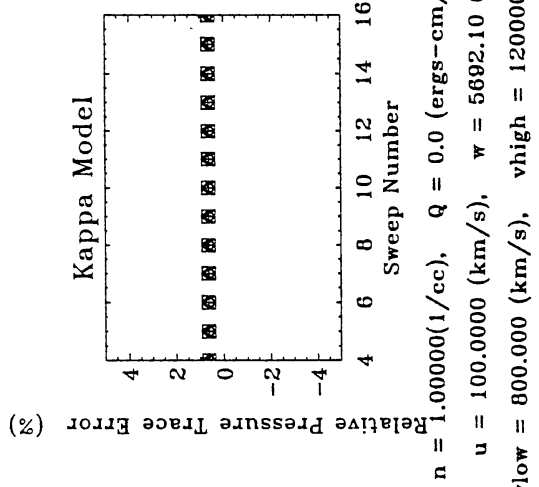


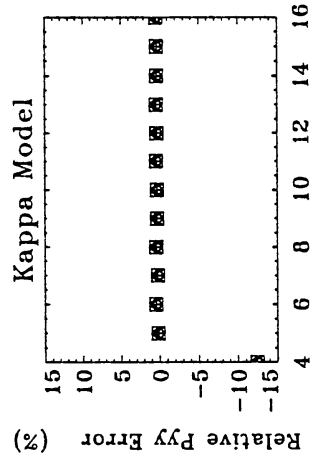


Fig. 18b.

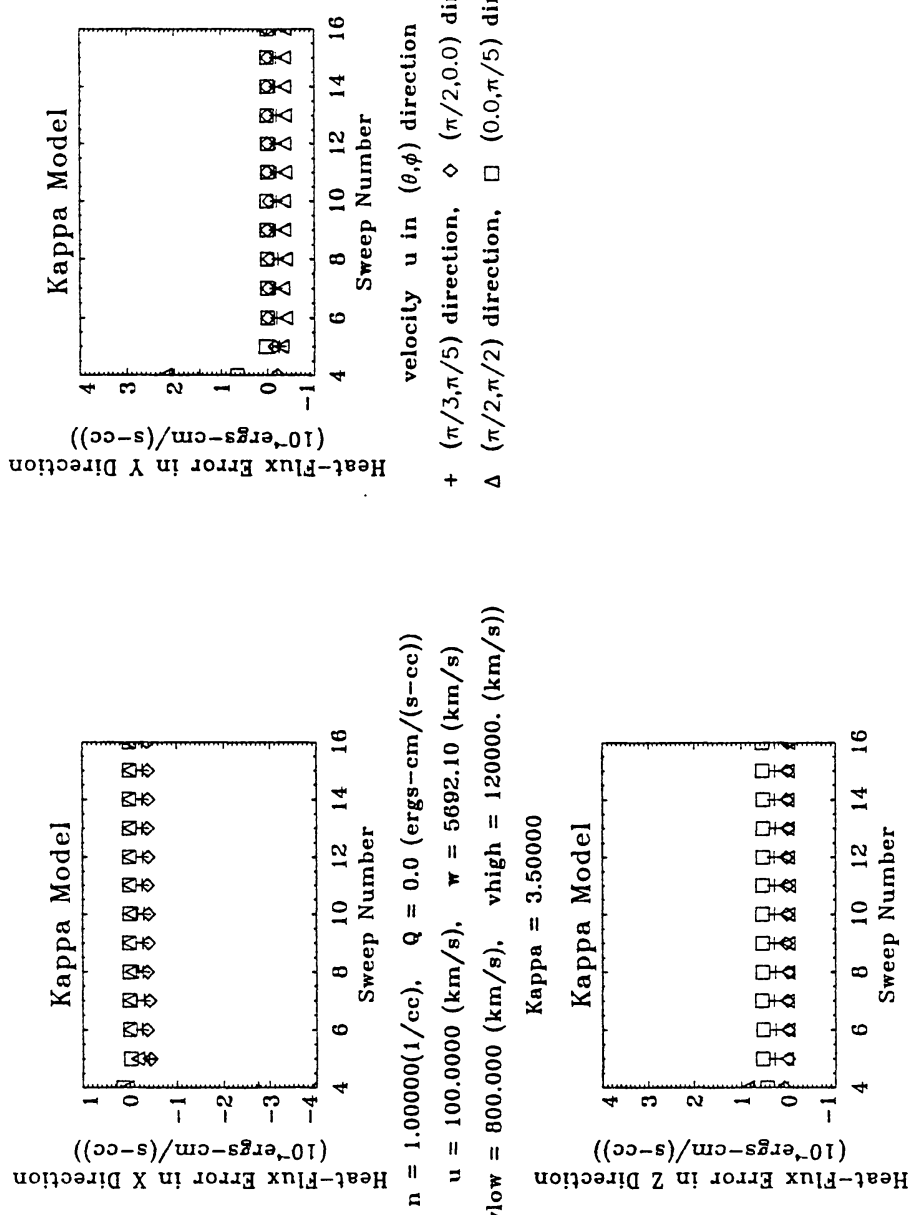


Fig. 18c.

$\langle E\rangle_k$ as defined above from the same data. The bow shock crossing at $\simeq 11:40$ and the magnetopause traversal ($\simeq 15:20$) are clearly delineated by this key parameter approach. Strong pressure anisotropy in trapped regimes causes this 'quick' determination of the mean energy via $\langle E\rangle_k$ to not be completely correct, but does reflect the distinct regime change in the mean energy of the gas as the magnetosphere is entered.

The second key parameter concerns the detection of structures in the loss or source cone and the particle energy where this was detected. For every PPA count rate accumulation by pitch-angle bins, there is a corresponding series in the Hydra telemetry of magnetic field polar angles that were used in that sort. From that series and the CODACON calibration, it is possible to compute the expected count distribution in the pitch-angle buckets for an isotropic distribution; an isotropic ambient distribution would correspond to a pitch-angle binned distribution strictly proportional to the number of $1\times 1^\circ$ pixels that view various pitch angles illustrated there. The key parameter index will say yes or no that there is statistically significant excess or depletion in the loss or source cones and what energy was being polled. Since not all energies are sampled sirnultaneously, knowing what energy was being polled will clarify the importance of the yes or no indication.

## 4.2. Production Quantities

### 4.2.1. *Moments*

High quality moments of the sampled distributions can be recovered in the following manner. Consider an integral number $N$ of energy sweeps for data acquisition of the phase space of a given charged component. As the interval occupied by the $N$ sweeps approaches the spin period, the samples of a given detector at a given energy sweep out a latitudinal belt in velocity space. Thus at fixed speed and detector's polar $\theta_j$ the azimuthal $\phi$ angular integration may be performed, viz.,

$$M_n(\{f(\mathbf{v})\}) \equiv \int_0^\infty v^2\,\mathrm{d}v \int_0^\pi \mathrm{d}\theta\sin\theta \int_0^{2\pi} \mathrm{d}\phi f(\mathbf{v}) W_n(v,\,\theta,\,\phi)\ .$$

$W_n$ is the weighting function peculiar to the moment in question. For the density, or 'zeroth' moment $W_0 = 1$; for the bulk speed $W_1 = \mathbf{v}$, a shorthand for three separate integrals for each Cartesian component. $W_2 = \mathbf{mvv}$, a shorthand for the momentum flux dyadic, etc. The $\phi$ integration exploits the periodicity and single valuedness of the $f(\mathbf{v})$ in the $\phi$ variable which is the angle about the spacecraft spin axis. This integral is done with cubic splines; the periodicity is used to obviate specifying leading and trail slopes to the integrand at the end points. The subsequent polar integration over $\theta$ is facilitated by the vanishing of the integrand at $\theta = 0,\,\pi$. This integral is also done with splines. The subsequent semi-infinite integral over speed is transformed by a change of variables that maps $[0,\,x) \to [0,\,a]$, where $a$ is a convenient finite dimensionless number consistent with the units and normalization

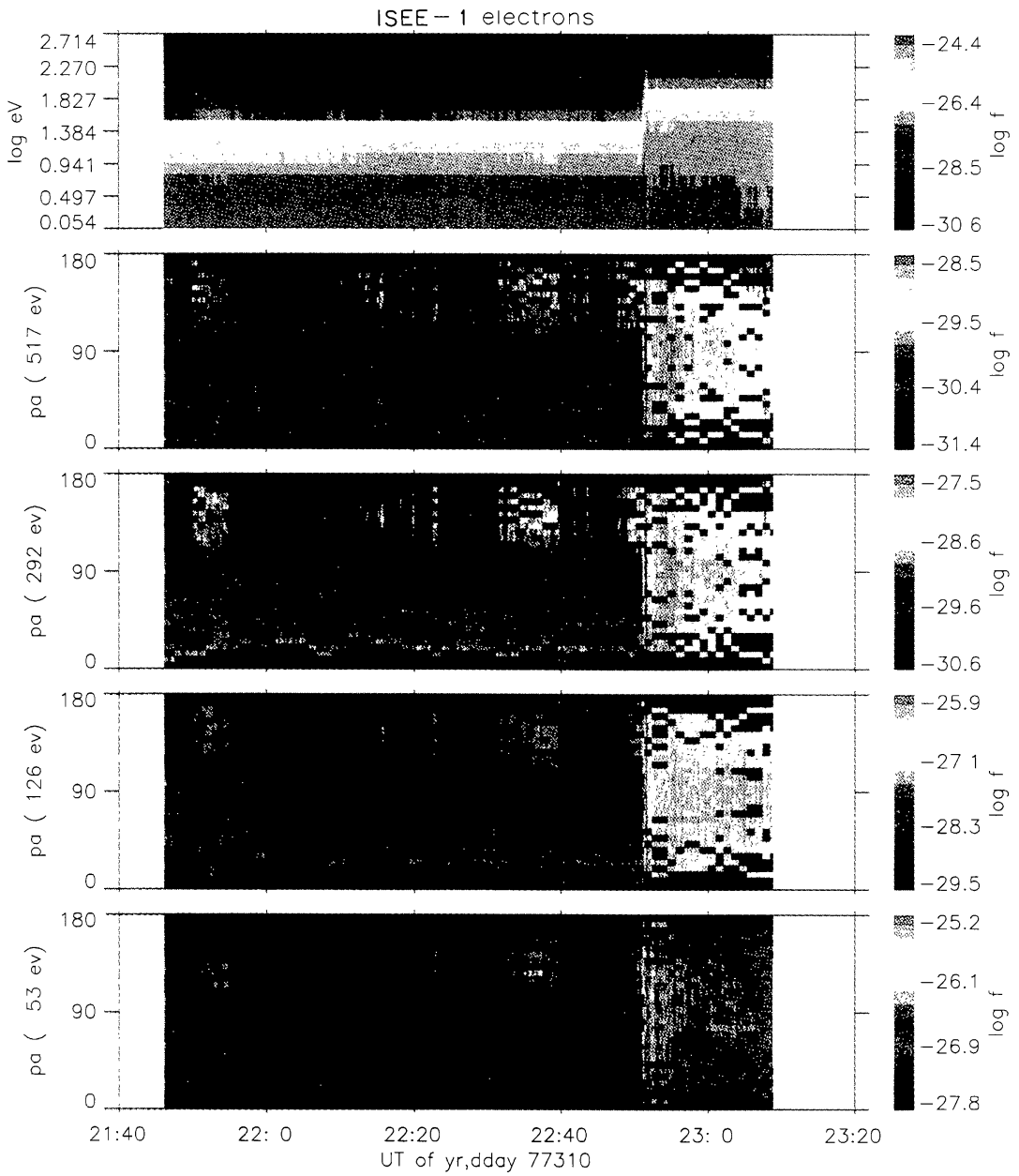


Fig. 19. Color Coded distribution function versus energy and pitch-angle distributions at selected energy versus time using ISEE proxy data. Black regions indicate no samples at the time of construction of spectro- gram. By software selection pitch angles can be 'filled' as implied by the underlying interpolation of $f(\mathbf{v})$ of the moments.

of $f$. Exploiting that $f(v \to \infty) \to 0$ and that the integrand vanishes at zero speed like $fv^{2+\epsilon}$, with $\epsilon \geq 0$, the triple integral can be completed in this way.

Figures 18(a–c) illustrates the recovery of the moments of a hot, subsonic kappa distribution appropriate for magnetospheric populations (cf. Binsack, 1966; Olbert, 1968, 1969; Vasyliunas, 1968; Christon *et al.*, 1989, 1991) using the HYDRA data collection scheme of alternate ion and electron energy sweeps as a function of the total number of sweeps of all species. After 4 or 5 interleaved sweeps the assumed

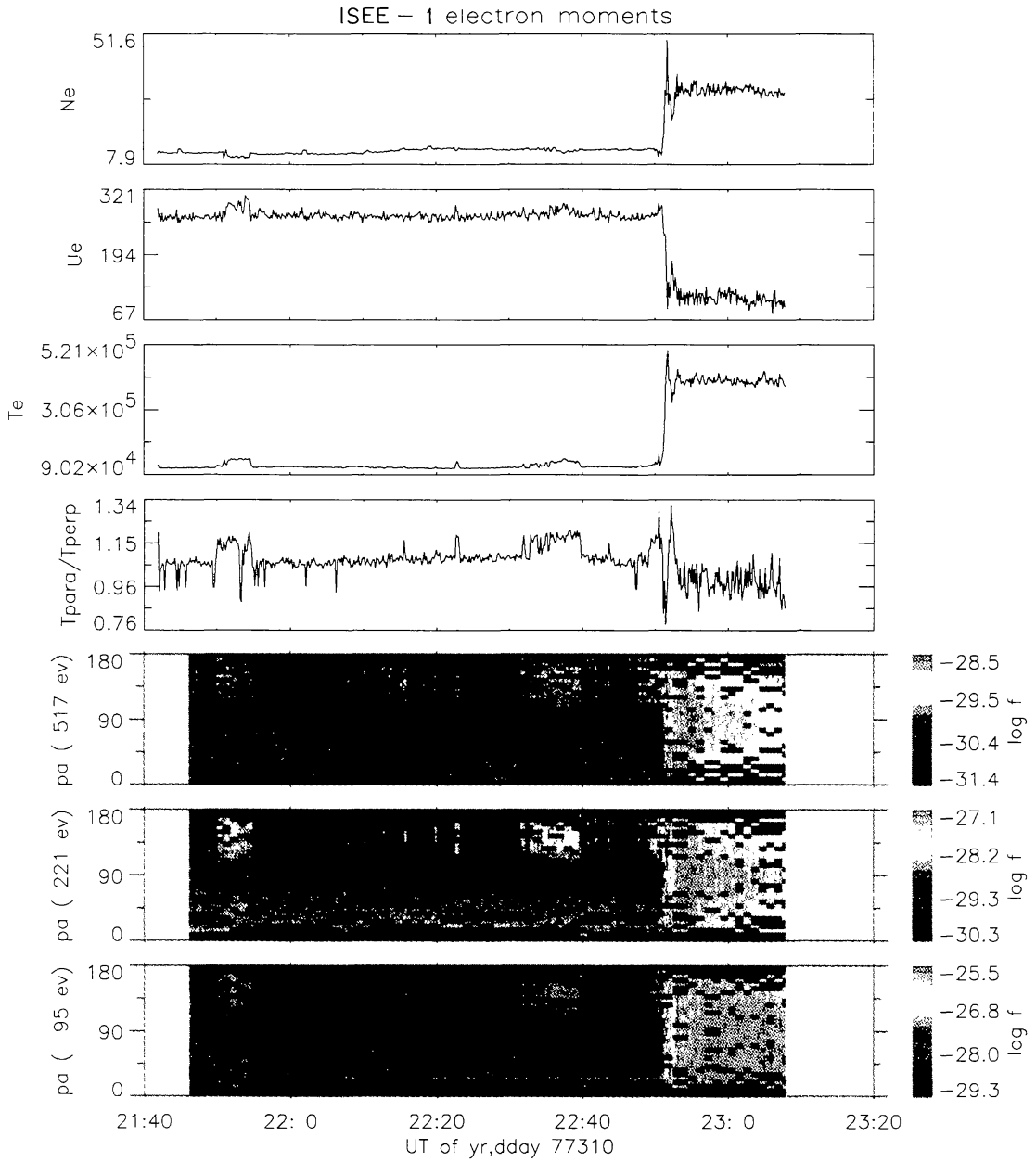


Fig. 20. Selected moments or key parameter proxys together with color coded spectrograms. ISEE-VES proxy data has been used for this illustration.

moments are recovered at generally better that the 1% level. Improved numerical integration techniques can improve these preliminary attempts even further. Typical energy sweeps per species occur with a period of 0.5 s, so that $N \simeq 6$ is comparable to the spin period.

### 4.2.2. *Color Coded Spectrograms*

As an example of other standard data products that will be produced for surveying the data, Figure 19 illustrates one of many possible formats that combines (using proxy ISEE data) spin averaged distribution functions vs energy (top panel) together

with pitch-angle distributions at selected energies below. This type of plot can be generated in real time at a work station of any of our co-I institutions with common team tailored software. The output can be tailored to the needs of the researcher before hardcopy is produced. These spectrograms can either be constructed from the raw data as here (with the attendent missing black pixels) or extended as implied in the interpolation that underlies the moment integrations.

Similarly, combinations of moment line plots, or their key parameter proxies. can be made with ancillary pitch-angle information at selected energies as in Figure 20.

4.2.3. *Distribution Functions in Gyrotropic Approximation Polar Plots*
For selected events isocontour pictures can be reconstructed using all possible sources of information including the PPA as in 15–16. These also can be combined with cuts of the distribution function along and orthogonal to the field as well as the reduced distribution functions of plasma dispersion theory.

## 5. Summary

The HYDRA experiment and team are ready to procede to the conclusion of our investigation. This paper demonstrates that we have built, calibrated and made extensive preparations for the deployment of this instrument and the interpretation of its data as a part of the GGS initiatives. Now we eagerly await its successful on-orbit turn-on sequence, having worked since 1978 to make that a reality.

## Acknowledgements

Clearly such a complex instrument could not have been constructed without the help of many hands. The science team would like to acknowledge the many occasions that our instrument manager Jack Millman of EER has been of assistance guiding our tortuous path toward spacecraft integration. The assistance of our experiment representative P. R. Harris, our surrogate PI, T. Palumbo and the experiment manager, R. Harten at GE/Martin is also appreciated. Numerous vendors have also made essential contributions to our experiment: Alan Lukemire and Art Ruitberg of Code 734 NASA GSFC were pivotal in our high and low voltage power supplies; George Lawrence of LASP designed and fabricated the Codacons for the PPA; Bill Morrow of Resonance Ltd. designed and fabricated our UV calibration lamp. Manuscript comments by Bob Holdaway are also appreciated. Figures 18(a–c) are provided by Chonghui Shen, a graduate student at the University of Iowa. We would also like to thank the NASA GSFC GGS Project Manager John Hrastar for his leadership in attempting to realize the POLAR mission in such difficult fiscal circumstances. Finally, we must acknowledge our debt to M. Acuna, the GGS Project Scientist for holding this ambitious program together against such unusal odds.

## References


Binsack, J.: 1966, 'Plasma Studies with the IMP-2 Satellite', MS Thesis, MIT.

Christon, S. P., Williams, D. J., Mitchell, D. G., Frank, L. A., and Huang, C. Y.: 1989, 'Spectral Characteristics of Plasma Sheet Ion and Electron Populations During Undisturbed Geomagnetic Conditions', *J. Geophys. Res.* **94**, 13409.

Christon, S. P., Williams, D. J., Mitchell, D. G., Huang, C. Y. and Frank, L. A.: 1991, 'Spectral Characteristics of Plasma Sheet Ion and Electron Populations During Disturbed Geomagnetic Conditions', *J. Geophys. Res.* **96**, 1.

Green, T. S. and Proca, G. A.: 1970, *Rev. Sci. Inst.* **41**, 1409.

Harvey, P. *et al.*: 1995, Space Sci. Rev. **71**, 583.

Herrero, F.: 1991, 'Light Trap Design Using Multiple Reflections and Solid Angle Attenuation: Application to a Spaceborn Electron Spectrometer', *Appl. Opt.* **31**, 5331.

Keller, J., Torbert, R., and Vandiver, J.: 1991, 'A High Speed Pitch Angle Sorter', *Rev. Sci. Inst.* **62**, 1353.

Mizera, P. F. and Fennel, J. F.: 1977, 'Signatures of Electric Fields from High and Low Altitude Particle Distributions' *Geophys. Res. Letters* **4**, 311.

Moore, T. E. *et al.*: 1995, Space Sci. Rev. **71**, 409.

Ogilvie, K. W., Scudder, J., and Doong, H.: 1978, 'The Electron Spectrometer on ISEE-1', *IEEE Trans. Geosci. Electronics* **GE-16**, 3, 261.

Ogilvie, K. W. *et al.*: 1995, Space Sci. Rev. **71**, 55.

Olbert, S.: 1969, in R. C. Carovillano. J. F. McClay, and H. R. Radoski (eds.), *Physics of the Magnetosphere*, D. Reidel Publ. Co., Dordrecht, Holland, p. 641.

Olbert, S., Egidi, A., Moreno, G., and Pai, L. G.: 1968, *Trans. AGU* **48**, 149.

Russell, C. T. *et al.*: 1995, *Space Sci. Rev.* **71**, 563.

Scudder, J. D., Sittler, E. C., Jr., and Bridge, H. S.: 1981, 'A Survey of the Plasma Electron Environment of Jupiter', *J. Geophys. Res.* **86**, 8157.

Vasyliunas, V. M.: 1968, 'A Survey of Low Energy Electrons in the Evening Sector of the Magnetosphere with OGO 1 and OGO 3', *J. Geophys. Res.* **73**, 2839.

Whipple, E. C.: 1978, '(U, B, K) Coordinates: A Natural System for Studying Magnetospheric Convection', *J. Geophys. Res.* **83**, 4318.